MISR Aerosol Product Attributes and Statistical Comparisons With MODIS

Ralph A. Kahn, David L. Nelson, Michael J. Garay, Robert C. Levy, Michael A. Bull, David J. Diner, John V. Martonchik, Susan R. Paradise, Earl G. Hansen, and Lorraine A. Remer

***Abstract*—In this paper, Multi-angle Imaging SpectroRadiometer (MISR) aerosol product attributes are described, including geometry and algorithm performance flags. Actual retrieval coverage is mapped and explained in detail using representative global monthly data. Statistical comparisons are made with coincident aerosol optical depth (AOD) and Angstrom exponent (ANG) retrieval results from the Moderate Resolution Imaging Spectroradiometer (MODIS) instrument. The relationship between these results and the ones previously obtained for MISR and MODIS individually, based on comparisons with coincident ground-truth observations, is established. For the data examined, MISR and MODIS each obtain successful aerosol retrievals about 15% of the time, and coincident MISR-MODIS aerosol retrievals are obtained for about 6%–7% of the total overlap region. Cloud avoidance, glint and oblique-Sun exclusions, and other algorithm physical limitations account for these results. For both MISR and MODIS, successful retrievals are obtained for over 75% of locations where attempts are made. Where coincident AOD retrievals are obtained over ocean, the MISR-MODIS correlation coefficient is about 0.9; over land, the correlation coefficient is about 0.7. Differences are traced to specific known algorithm issues or conditions. Over-ocean ANG comparisons yield a correlation of 0.67, showing consistency in distinguishing aerosol air masses dominated by coarse-mode versus fine-mode particles. Sampling considerations imply that care must be taken when assessing monthly global aerosol direct radiative forcing and AOD trends with these products, but they can be used directly for many other applications, such as regional AOD gradient and aerosol air mass type mapping and aerosol transport model validation. Users are urged to take seriously the published product data-quality statements.**

***Index Terms*—Aerosols, Moderate Resolution Imaging Spectroradiometer (MODIS), Multi-angle Imaging SpectroRadiometer (MISR), remote sensing.**

Manuscript received February 12, 2009; revised April 1, 2009. First published September 15, 2009; current version published November 25, 2009. This work was supported by the National Aeronautics and Space Administration (NASA) Climate and Radiation Research and Analysis Program under the Atmospheric Composition Program and the Earth Observing System–Multi-angle Imaging SpectroRadiometer (EOS-MISR) Project. The work of R. A. Kahn was supported in part by the NASA Climate and Radiation Research and Analysis Program under H. Maring and NASA Atmospheric Composition Program under P. DeCola and EOS-MISR project.

R. A. Kahn and L. A. Remer are with the Laboratory for Atmospheres, NASA Goddard Space Flight Center, Greenbelt, MD 20771 USA (e-mail: Ralph.Kahn@nasa.gov).

D. L. Nelson and M. J. Garay are with Raytheon Intelligence and Information Systems, Pasadena, CA 91101 USA.

R. C. Levy is with Science Systems and Applications, Inc., Lanham, MD 20706 USA, and also with the NASA Goddard Space Flight Center, Greenbelt, MD 20771 USA.

M. A. Bull, D. J. Diner, J. V. Martonchik, S. R. Paradise, and E. G. Hansen are with the NASA Jet Propulsion Laboratory, Pasadena, CA 91109 USA.

Color versions of one or more of the figures in this paper are available online at http://ieeexplore.ieee.org.

Digital Object Identifier 10.1109/TGRS.2009.2023115

I. Introduction

SPACEBORNE Earth-orbiting instruments make it possible to monitor conditions over the entire planet, a capability of increasing importance as questions about climate change gain urgency. Since the advent of the global Earth observation era, vast amounts of data have been collected and processed into records related to geophysical quantities.

Satellite-derived geophysical quantities are typically aggregated into statistical summaries aimed at characterizing current environmental conditions and revealing trends, whereas subsets of these data are studied for the information they yield about specific natural and anthropogenic events. In many cases, a detailed understanding of the strengths and limitations of the derived quantities is central to the application. However, the retrieval algorithms for many of these newly derived quantities are quite complex, and at present, the algorithms continue to be refined, based partly on the results obtained during field campaigns and other validation exercises. In addition, techniques for assessing and for reporting the meaning, quality, and uncertainty of the results are still developing.

The Multi-angle Imaging SpectroRadiometer (MISR) aerosol product [1] falls into this category. The product has been used with considerable success to retrieve aerosol optical depth (AOD) over land and water [2]–[13], aerosol type [14]–[17], aerosol radiative forcing [18]–[21], and aerosol plume height [16], [22]. However, some of the retrieval products are still being refined, and some aspects of the products have not yet been fully described in the literature.

This paper fills several key gaps in the published work describing MISR aerosol product attributes and performance, and provides links between MISR and MODIS aerosol products. It begins with descriptions of MISR product-sampling characteristics, retrieval-algorithm approach, and retrieval quality information reported in the Level-2 Standard aerosol product (MIL2ASAE). Comparisons are then made with the Standard aerosol product from MODIS, which flies aboard the Terra satellite with MISR. MODIS is a single-view multispectral imager, having a wide swath that encompasses the MISR field of view (FOV). The MODIS aerosol product [23], [24] is increasingly being used in conjunction with MISR, as the greater MODIS coverage and shorter revisit time complement the particle microphysical property information, and retrievals over bright desert and over ocean regions excluded by glint in the near-nadir view, provided by MISR [25]. This paper concludes with a summary of product performance, implications for using MISR aerosol products in scientific applications, and reflections on some other published assessments of these products.

II. MISR Product Geometric Attributes and Aerosol Retrieval Coverage Analysis

MISR was launched aboard the NASA Earth Observing System's Terra spacecraft in December 1999 into a Sun-synchronous orbit that crosses the equator at about 10:30 A.M. local time, descending on the dayside of the planet. The subspacecraft point reaches to about 82° latitude. The orbit number is a sequential counter related to the time of data acquisition; about 14.56 orbits are completed each day, which amounts to about 5315 orbits per year.

MISR has nine cameras pointed toward the Earth at nine look-angles ranging from $+70°$ through nadir to $-70°$ along the spacecraft ground track. Each camera focal plane contains four line arrays of 1504 photoactive pixels each, which have blue, green, red, and near-IR filters [26]. The instrument images reflected sunlight, covering equatorial latitudes about once in nine days and polar latitudes about once every two days.

A. Geometry of the Level-1B2 Calibrated Radiance and Level-2 Aerosol Products

MISR produces 36 simultaneous images (nine angles, at each of four wavelengths); cross-track spatial sampling is 250 m for the nadir camera and 275 m in the off-nadir cameras. Along-track instantaneous sampling varies from about 214 m at nadir to 707 m for the most oblique cameras, but sample spacing is maintained at 275 m, so the data are resampled to an effective resolution of 275 m in all cameras, are coregistered onto the World Geodetic System 1984 Earth ellipsoid, and projected onto a common space-oblique Mercator grid [26]. Over land, the data are, in addition, projected onto a digital elevation model to account for terrain effects. These steps are part of the initial (Level 1) processing [27], which includes both geometric and radiometric calibration; the calibrated radiance product is designated Level 1B2 (L1B2). The MISR aerosol parameters, derived primarily from L1B2 radiances, are part of the MISR Level-2 Aerosol-Surface (L2AS) product. In total, the Standard MISR L1B2 ellipsoid-projected radiance product for a single orbit is about 2.3 GB in size and the corresponding MISR L2AS product is between 20 and 33 MB.

The locations of Terra orbits are designated by path numbers; a "Path" is a strip, following the satellite orbit track nearly from pole to pole, and fixed geographically to the Earth's surface. There are 233 paths covering all the unique spacecraft tracks flown by Terra over its 16-day orbital repeat cycle. Key aspects of MISR coverage and aerosol product geometry obtained on a single orbit are shown in Fig. 1. The MISR swath is a data structure comprised of 180 blocks, each 140.8-km along-track and 563.2-km cross-track, on the daylit side of the orbit. Blocks are numbered consecutively from north to south (as MISR orbits north to south on the dayside of the planet); block 90 is near the equator. Only about 142 blocks are actually sunlit during any given orbit, and these blocks change with the seasons. No MISR imaging data are acquired for the blocks in darkness, which are called *End Blocks*. In the standard "Global" imaging mode, which is obtained whenever MISR is on the dayside of the Earth, the four spectral channels for the nadir view and the red band in the other eight cameras (12 channels in total) are acquired at full 250–275-m resolution, and for the remaining 24 channels, 4×4 pixels are averaged onboard to a single value, so the resulting radiances for these channels are reported on 1.1-km resolution "subregions" (Fig. 1). For "Local" mode, which must be requested and programmed in advance of acquisition, all 36 channels are obtained at full 250–275-m resolution, for the entire swath width and for 300 km along-track.

Each block in the data structure is 563.2 km in the cross-track direction; however, the region actually within the FOV depends on camera view angle and spacecraft orientation, and is limited in overall width to about 420 km for the off-nadir cameras and about 382 km for the nadir view. Toward the swath edges, pixels are imaged in fewer than nine cameras due to differences in camera optics and the Earth's rotation. For the purposes of this paper, we define "*InFOV*" as an approximate quantity that includes only regions fully within the nadir camera FOV, as nearly all the nadir pixels are within the FOV of every other camera. Pixels in the remaining swath area are designated *Edge Pixels*. Table I provides definitions of some terms used in this paper and in the MISR Standard products.

Achieving sufficient processing efficiency to cope with the large (2.3 GB/orbit) data stream and limiting final product data volume are among the challenges of designing the MISR Level-2 aerosol-retrieval algorithm. In part to reduce processing load and product volume, MISR aerosol retrievals are performed on regions comprised of 16×16 1.1-km subregion patches, which yield an effective aerosol product horizontal resolution of 17.6 km (Fig. 1). Table II summarizes MISR coverage for January 2006. Within the swath data structure, about 60% of regions are *InFOV*, when *End Blocks* and *Edge Pixels* are taken into account. As discussed in detail in Section II-B below, other considerations determine which regions, about 15% of the total *InFOV*, ultimately produce successful aerosol retrievals. (For a retrieval to be successful, the Level-1 radiances must pass all the initial data-quality tests, as covered in Section II-B, and at least one aerosol model in the algorithm climatology must pass all the acceptance criteria, as described in [28]).

MODIS data for each orbit are divided into granules representing 5-min orbit segments, similar to MISR blocks, but much larger, encompassing the full MODIS swath, about 2300 km in width. Each Level-1 pixel is tagged with its center latitude and longitude. MODIS aerosol retrievals are performed on regions comprised of multispectral observations taken at 250 or 500 m, depending on spectral band [23], [24]. MODIS aerosol-retrieval regions (also called frames) are 10 km $\times$ 10 km at the swath center and become progressively elongated away from the center of the ground track. In the cross-track dimension, a Level-2 product granule contains 135 samples, and in the along-track dimension, a granule typically contains 203 across-track scan lines.

The MISR swath intersects approximately the middle 40 of the 135 MODIS regions across a MODIS swath. Fig. 2 shows, with retrieval region centers, the coincident coverage over part of a Terra orbit. MISR and MODIS pixels have different spatial

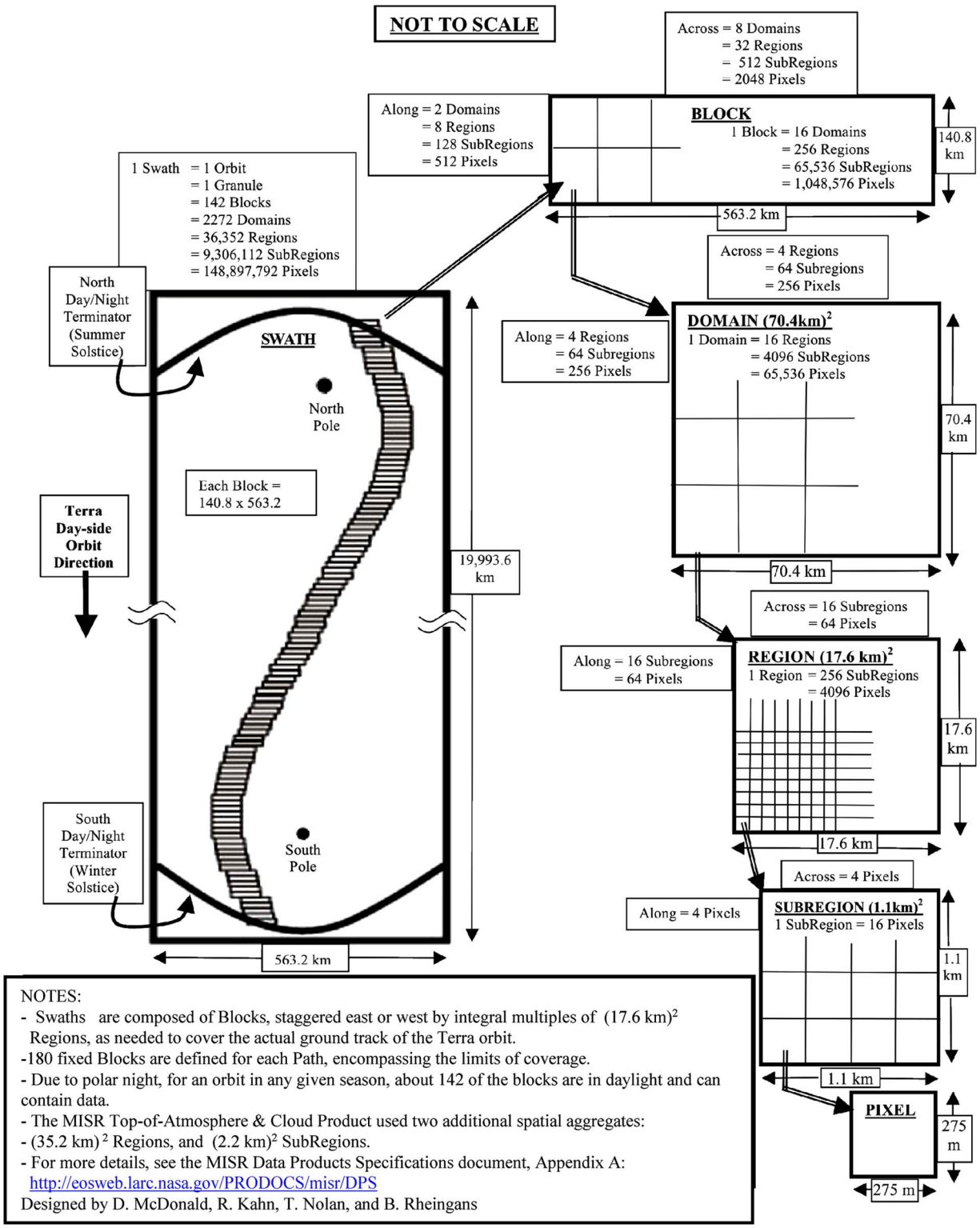

Fig. 1. Schematic hierarchy of MISR Aerosol-Surface product spatial domains.

resolution and sample spacing, and are projected onto different grids. To facilitate comparisons between MISR and MODIS observations, we define a common geographic grid having uniform, 4 km spacing, that over-samples the regions of both products. This effectively subsamples the 17.6-km MISR and 10-km MODIS regions over which retrieved values are reported, so higher spatial sampling would provide no additional information. About six grid points fall into a MODIS aerosol-retrieval region and about 19 into a MISR region. With the underlying assumption that the retrieved values represent the entire 17.6- or 10-km retrieval region for MISR and MODIS, respectively, statistical comparisons made at the grid points amount to symmetric equal-area weighting of the MISR and MODIS results.

TABLE I
SOME TERMS USED HERE AND IN THE MISR AEROSOL PRODUCTS (VERSION 22 AND BELOW)

Field	Parameter Value used here	Parameter Value used in MISR L2AS V22 and below	Explanation
RegClassInd	*RegionPasses*	*Clear*	Retrieval region that passes all the *RegClassInd* tests
RegClassInd	*No Radiance and/or Geometry Data, or NoSubregPass*	*None Valid*	Either outside the area imaged, or no subregions in this region pass all tests required to attempt retrieval
RetrAppMask	*InFOV*	[Not] *Fill*	Subregion in the MISR product structure is within the camera field of view
RetrAppMask	*SubregionPasses*	*Clear*	Subregion that passes all the *RetrAppMask* tests
RetrAppMask	*InFOV Not Suitable*	*Not Suitable*	For this paper, only subregions eliminated due to *Missing Geometry, Oblique Sun, or Topographic Complexity* are counted here
AerRetrSuccFlag	*No Attempt Made*	*No Attempt Made + Fill*	These are both situations where retrieval was not attempted. *Fill* simply means the region was eliminated before the Table III and IV tests were performed.
AerRetrSuccFlag	*No Match*	*No Match + Default Surface Attempt*	These are both situations where the algorithm finds no match. *Default Surface* simply means a surface retrieval was attempted using a default AOD value.

TABLE II
MISR (VERSION 22) AND COINCIDENT MODIS/TERRA (COLLECTION 5) AEROSOL RETRIEVAL COVERAGE STATISTICS FOR JANUARY 2006

Quantity	Value
Number of orbits	439
Total number of MISR regions in data structure	20,229,120
Total number of *InFOV* MISR regions	12,078,720
Percent of MISR regions *InFOV*	59.7
Percent of MISR *InFOV* regions resulting in AOD retrievals	14.6
Total number of MODIS regions in MISR FOV *(approx.)*	34,955,000
Percent of MODIS "Average" AOD Retrievals in entire MISR swath	13.7
Percent of MODIS "Best" AOD Retrievals in entire MISR swath	13.3

B. MISR Aerosol (L2AS) Product Coverage

The MISR aerosol-retrieval algorithm itself can be divided into three stages [28]. Stage 1 involves preprocessing the L1B2 radiances, performing out-of-band spectral, ozone, and water vapor absorption corrections. In addition, screening is performed in Stage 1, flagging first on a region-by-region-basis missing radiance data and geometric parameters, complex terrain over land, and low solar zenith angle cases, then identifying, subregion by subregion, additional missing radiance data, Sun-glint-contaminated views over water, cloudy locations, and other questionable conditions, and, finally, converting radiances to equivalent reflectances. In Stage 2 of the processing, the type of algorithm used to perform the retrieval (land or water) is determined based on the remaining subregions that pass the Stage 1 tests. Finally, in Stage 3, acceptance criteria are used to identify simulated top-of-atmosphere-equivalent reflectances that match those observed. Because MISR aerosol product coverage depends primarily on the screening in Stage 1, this screening is described in detail in this section.

Results of the tests performed in Stage 1 of the retrieval algorithm are recorded in the regional classification indicator (*RegClassInd*) and the retrieval applicability mask (*RetAppMask*), which are included in the aerosol product. The tests are done in a fixed sequence, and the values of *RegClassInd* and/or *RetAppMask* are set to indicate the first test that a region or subregion fails, respectively. If a region or subregion fails one of these tests, no further tests are performed on that data element; whether a particular region or subregion would fail subsequent tests is undetermined. A detailed accounting of allowed output parameter values, as encoded in the MISR Standard aerosol product, is given in the MISR Data Product Specification document [29], and the underlying procedures are described in the Level-2 Aerosol Retrieval Algorithm Theoretical Basis document [28]. These documents are updated periodically as the algorithm evolves, and configurable parameters that alter the performance of some tests are reported in the product data files themselves. In this paper, we concentrate on overall outcomes for Version 22 of the algorithm, the current operational version, which has been used to reprocess the data for the entire MISR mission.

Table III lists, in the sequence they are performed, the *RegClassInd* test results for the 439 orbits of January 2006. For about 12% of the regions designated *InFOV*, at high latitudes, large solar zenith angles invalidate the planar-atmosphere assumption used by the Standard aerosol-retrieval algorithm. Nearly 50% of the regions are eliminated by subsequent tests that excluded all subregions (see Table III footnote), leaving 39% of the *InFOV* regions for further analysis.

The *RetAppMask* subregional test results are summarized in Table IV. These tests are performed independently on each camera and band, as appropriate; for example, data could be missing for a single spectral band or sun glint might contaminate just a few cameras. A subregion might not be excluded if only a few channels are removed. As the *RetAppMask* tests are performed sequentially, once a subregion is eliminated by a test, it is added to the count for that test, and no subsequent tests are performed on it. The numbers reported in Table IV are approximate percentages of all *InFOV* subregions eliminated by the test indicated.

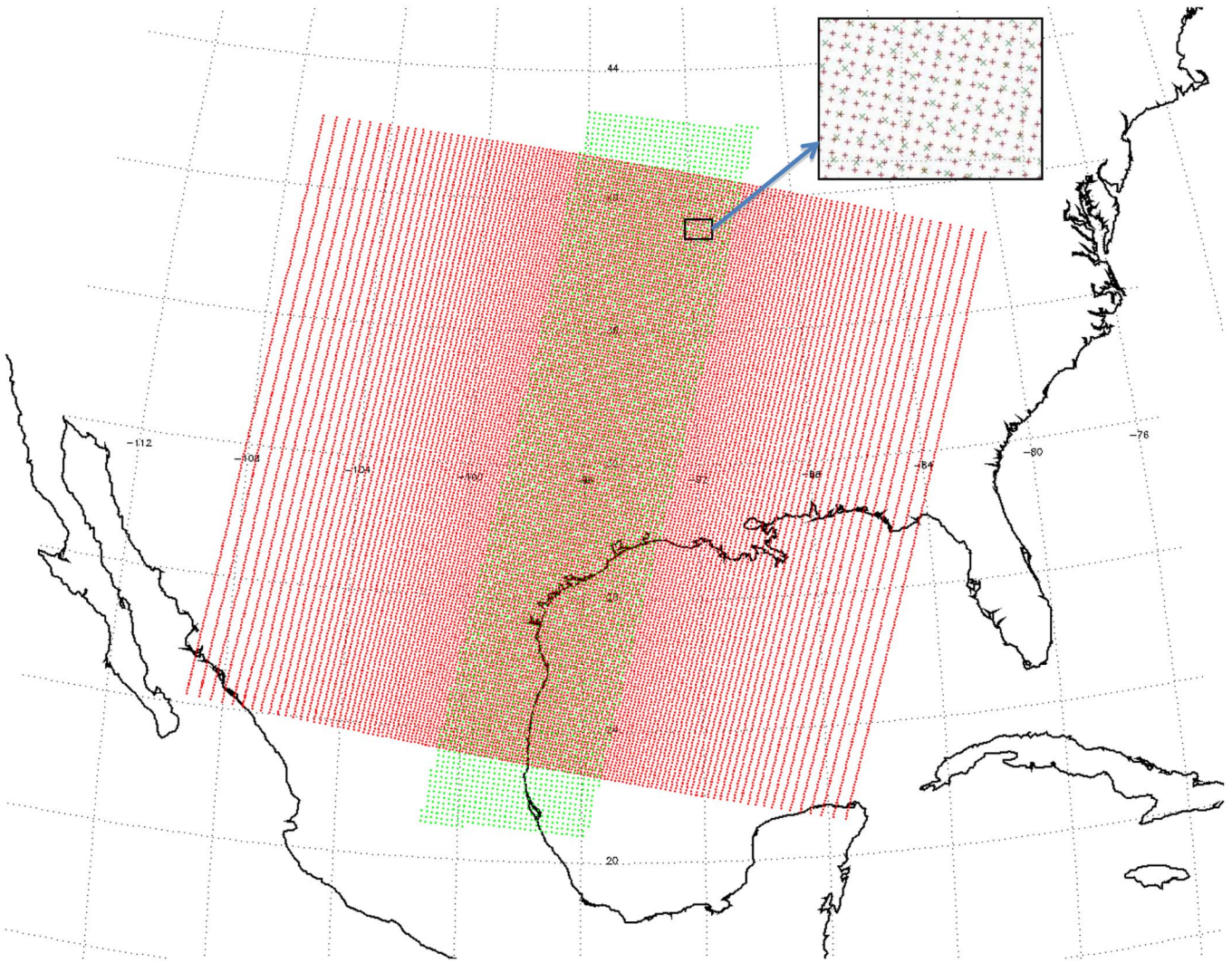

Fig. 2. Example of MISR and MODIS relative colocated coverage. Red dots represent the centers of 10-km MODIS aerosol-retrieval regions. Green dots represent the centers of MISR 17.6-km retrieval regions. (Note that all MISR region centers are plotted, not just those *InFOV*.) This data sample covers MODIS granule A2006001.1717.005 and part of MISR Orbit 32130, Path 26. The inset provides an expanded view, showing the relationship between individual MISR (green) and MODIS (red) region centers.

TABLE III
MISR AEROSOL PRODUCT (VERSION 22) *RegClassInd* RESULTS FOR JANUARY 2006, FOR *InFOV* GRID POINTS* ONLY

***RegClassInd* Outcome Parameter**	**Approximate Percent**
***No Radiance and/or Geometry Data*†**	0.0
Oblique Sun (generally high latitudes)	11.8
Topographically Complex (generally mountainous areas)	0.2
***NoSubregPass*†**	49.5
Region Passes	38.5

*For the purposes of this paper, "*InFOV*" is defined as an approximate quantity, which includes only fully viewed regions within the nadir camera imagery.

†The parameter *None Valid* in the *RegClassInd* (see Table I) is set when there is no image data in a region. At the end of Stage 1 processing, if all subregions in a region have been eliminated for any reason, the region is added to the count for the *None Valid* parameter. The percentage of *No Radiance and/or Geometry Data* has been set to 0 in this accounting, as the edge pixels are not included in the *InFOV* estimate.

In the previous testing step, *RegClassInd* removed 12% of *InFOV* subregions for all channels (Table III). Between 0% and 1% is topographically obscured, meaning that the line-of-sight of a camera is blocked by intervening topography; this generally affects only the most obliquely viewing cameras. Glint contaminates about 8%–25% of the remaining *InFOV* subregions for individual camera views, with the near-nadir views most commonly affected. When all the *RegClassInd* tests, which eliminate entire regions, as well as the individual-channel *RetAppMask* removals to this point are taken into account, nearly 45% of *InFOV* subregions have been excluded for aerosol retrievals, due mainly to algorithm physical requirements, preferentially at high latitudes and near swath edges.

Most of the remaining tests that eliminate significant data are cloud related. As might be expected, clouds have a larger effect at more oblique viewing angles, due to the combined effects of increased atmospheric path length, which makes optically thinner clouds more detectable, and of 3-D cloud structure [30]. The aerosol cloud-screening tests include the three MISR

TABLE IV
MISR AEROSOL PRODUCT (VERSION 22) *RetAppMask* RESULTS FOR JANUARY 2006, REPORTED AS AN APPROXIMATE PERCENT OF ALL *InFOV* SUBREGIONS REMOVED BY THE TEST INDICATED

***RetrAppMask* Outcome Parameter**	**Approximate Percent[§]**
InFOV Not Suitable – this includes all subregions within regions than were eliminated by the *RegClassInd No Radiance Data, Oblique Sun*, and *Topographically Complex* tests (see Table III)[†]	12.0
Missing Data – outside camera FOV or data gap	6.9 to 8.4
Topographically Obscured – angular view blocked by topography	0 to 1.1
Glint Contaminated (varies with camera view angle)	8.2 to 25.0
Topographically Complex	0
Poor Quality (based on Level 1 radiometry quality test)	0 to 1.1
Cloudy (based on MISR Standard radiometric camera-by-camera, stereo-derived, and angular-signature cloud mask logic)	29.7 to 39.2
Too Bright – exceeds radiance threshold	2.0 to 3.9
Not Smooth – radiance angular smoothness test failed	1.4 to 2.1
Not Correlated – angular image correlation test failed	5.7 to 7.4
Cloudy Other Camera – rejected because another camera was set to "cloudy"	1.4 to 4.3
Bright Other Camera – rejected because another camera was set to "too bright"	0.3 to 1.0
Subregion Passes	7.9 to 12.0

[§]These subregion parameter values are camera and band-specific (up to 36 distinct values). The range is given here. A subregion can be used for retrieval if at least four cameras are not flagged; over land, a combination of steep and less steep views is also required. Retrieval will not be attempted with the over-dark-water algorithm for any region having fewer than 32 passing subregions; 16 subregions are required over land. The results of the # Cameras and # Subregions Passing tests are added to the *No Attempt Made* parameter in *AerRetrSuccFlag* (see Table V), but do not appear in the *RetAppMask*.

[†]In the MISR product, *Not Suitable* includes *Edge Pixels*. Here 25% was subtracted from the value in the MISR Standard product, to approximately remove *Edge Pixels* from the count.

TABLE V
MISR AEROSOL PRODUCT (VERSION 22) AEROSOL-RETRIEVAL SUCCESS FLAG (*AerRetrSuccFlag*) RESULTS FOR JANUARY 2006, FOR *InFOV* GRID POINTS ONLY

***AerRetrSuccFlag* Outcome Parameter**	**Approximate Percent**
No Attempt Made – *InFOV* regions eliminated by *RegClassInd* tests, or no subregions remain after *RetrAppMask* tests[†]	81.1
No Match – among the regions where *retrieval was attempted*, the algorithm aerosol mixture table does not produce any good matches to observed radiances[§]	22.8
Successful Retrieval – among the regions where a *retrieval attempt was made*	77.2
Overall Successful Retrieval – among all *InFOV* regions	14.6

[†]This is the sum of the *No Attempt Made* and *Fill* values in the MISR Standard product (see Table I for details). The count incorporates the explicit *RetrAppMask* test results (Table IV), as well as several tests that affect small numbers of additional subregions, such as the Shallow Water exclusion test and the SUFFICIENT CONTRAST TEST over land. It also reflects the results of the # Subregions Passing requirement (see Table IV footnote).

[§]This is the sum of the *No Match* and *Default Surface Attempt* values in the MISR Standard product (see Table I for details). About 2.2% of the values reported here are filled for a *Default Surface Attempt* in the January 2006 data.

standard cloud masks (radiometric camera-by-camera cloud mask, stereo-derived cloud mask, and angular-signature cloud mask) [1], which eliminate about 35% of the remaining subregions. Two additional tests for angular smoothness and pixel correlation are also performed [31], which tend to identify heterogeneous scene elements such as cloud edges, and between them, remove another 8% of the subregions. The cloud-mask logic includes more stringent tests for clouds over snow and ice [28]. However, aerosol retrievals *are* attempted over such surfaces if they pass these cloud tests. Several further tests, dealing with contingencies such as shallow water and insufficient contrast over land [28], remove some additional subregions but are not reported explicitly in the *RetAppMask* (although shallow water is identified in the *RegSurfTypeFlag* parameter [29]).

Taken together, about 10% of subregions remain after all tests. However, the algorithm will attempt a retrieval for an over-land region if just 16 of 256 subregions pass all tests. If the land retrieval is not attempted or fails, the algorithm determines whether the criteria for performing a water retrieval are met; this can also occur, for example, over sufficiently large inland bodies of water that pass the "shallow-water" exclusion. Over water, at least 32 subregions are required for the algorithm to attempt a retrieval; the looser constraint over land is a practical matter—it increases coverage without significantly affecting over-land retrieval quality. Therefore, although about 10% of the subregions remain after all tests, retrievals are attempted on almost 20% of *InFOV* regions (Table V).

The screening process described earlier represents an effort to identify only the most suitable radiance data upon which to perform aerosol retrievals. As they must be applied uniformly to the entire global data stream, the test criteria inevitably strike a compromise between maximizing coverage and achieving confidence in data quality. The labor- and computation-intensive MISR research aerosol-retrieval algorithm [32] has demonstrated that if pixel patches are selected manually and processed individually, then additional retrievals can be squeezed from MISR radiance data in some circumstances. However, most applications of MISR aerosol products rely on having frequent large-scale coverage that only the Standard algorithm can provide. Further refinement of the operational radiance data-selection process is likely to produce incremental additional

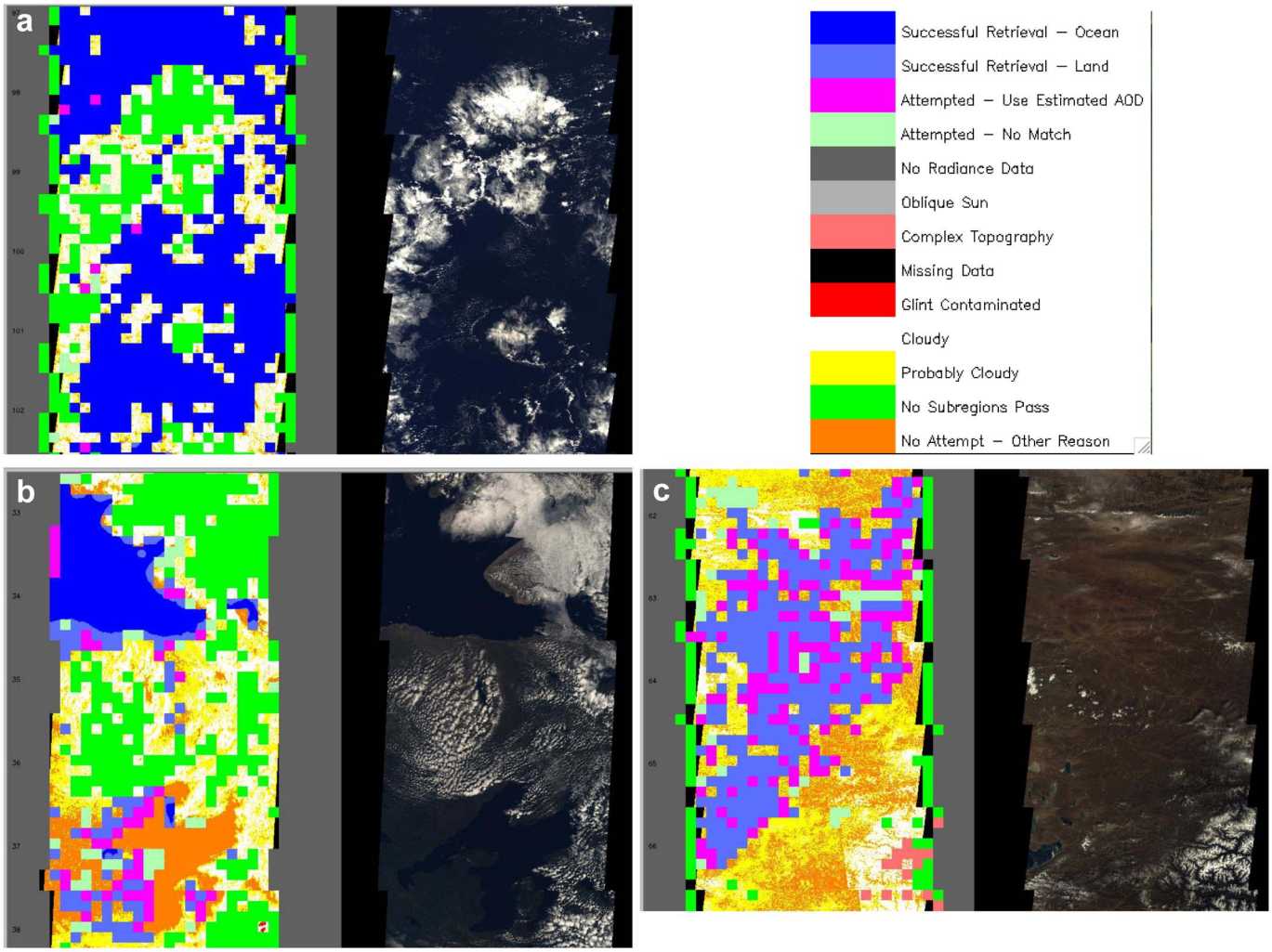

Fig. 3. Maps showing the distribution of retrieval status, with paired nadir-view true-color images. (a) Orbit 35117, Path 53, Blocks 97–102, July 25, 2006, ocean scene with cloud in the central Pacific, centered near 11.3 S latitude, 147.4 W longitude. (b) Orbit 35117, Path 53, Blocks 33–38, mixed ocean, land, and cloudy scene in northern Canada, centered near 67.9 N latitude, 119.2 W longitude. (c) Orbit 32501, Path 137, Blocks 62–66, January 27, 2006, land scene on the Tibetan Plateau, with cloud and some complex terrain, centered near 33.2 N latitude, 93.1 E longitude. Note that some factors remove individual subregions, whereas others remove entire regions.

coverage. However, the overall coverage envelope is set by instrument spatial coverage and resolution, retrieval-algorithm physical requirements, and natural scene heterogeneity, including cloud occurrence.

Table V summarizes overall Version 22 algorithm performance for January 2006; of the regions for which retrievals were attempted, 77% produced successful results, which amounts to about 15% of all *InFOV* regions. These results vary with season; for *InFOV*, successful retrievals range from about 15%–19%, with the peak in northern spring and summer, when overall AOD is highest globally.

Fig. 3 shows the geographic distribution of successful MISR retrievals over ocean (dark blue) and land (light blue) and shows, in an approximate manner, locations where specific data-quality criteria were not met, under some typical conditions. This representation cannot be exact because, where subregions are eliminated, there are often multiple contributing factors that each eliminates data from one or more of the 36 spectral angular channels. As a result, mixed-cause eliminations can fall into any of several classes.

An effort has been made to define classification rules used for the maps shown in Fig. 3 that give fair indication of primary causes, to the extent possible. The "*No Radiance Data*" gray strips on either side of the swaths are edge pixels, areas within the MISR orbit data structure but outside the FOV (Table II). Most of the "missing-data" locations are also near the swath edges (Table IV; black in Fig. 3). Subregions within a cloudy region can be eliminated by any of several tests, so such locations are sometimes designated "*Cloudy*" (white, based on the *RetAppMask* values for the 70° forward and aft cameras in these illustrations), "*Probably Cloudy*" (yellow, which aggregates *RetAppMask* designations "*Too Bright*," "*Not Smooth*," "*Not Correlated*," and "*Cloudy Other Camera*" in Table IV, again using the 70° forward and aft cameras), or "*No Subregions Pass*" (dark green), as shown in Fig. 3(a). Over barren land [Fig. 3(c)], "*Complex Topography*" (pink) eliminates a few regions; other locations are removed as a result of cloud, including small clouds difficult to see in these images. Locations where insufficient subregions remain in a region, due to some combination of factors listed in Table IV, as well as other considerations such as

shallow water and low surface contrast over land, are designated "*No Attempt—Other reason*" (brown). Fig. 3(b) shows masking and retrieval performance in an area containing land, water, shallow water, and coast. At a few locations near the land–water boundary in this scene, retrievals were attempted but resulted in "*No Match*" (light green), meaning that the retrieval was unable to fit an existing aerosol model to the observed equivalent reflectances. "*Oblique Sun*" is found at high latitudes. Finally, due to the Sun-synchronous 10:30 A.M. equator-crossing Terra orbit, when "*Glint*" eliminates up to five cameras, it is usually toward the east edge of the swath. (Oblique-Sun and glint situations do not happen to appear in the cases selected for Fig. 3.) Further elaboration of these tests is provided in [29] and [28].

As MISR is an imager, there is information in the spatial distribution of retrieved aerosol types that, in some cases, can be used to select an aerosol type for nearby retrieval regions where some aspect of the retrieval itself failed, and can therefore help fill in AOD values (for details, see optical-depth defaults [28, Sect. 3.5.7]). These cases are flagged and are identified as *Default Surface Attempt* in the *AerRetrSuccFlag*; they are included in the *No Match* category of Table V and are colored purple in Fig. 3. However, these values are reported in the *RegSfcRetrOptDepth* field of the MISR Standard aerosol product, and their quality is sufficiently high that they can be used for surface retrievals. In the *RegBestEstimateSpectralOptDepth* field, gaps in successful retrieval coverage are filled using a 3×3 average of neighboring region AOD values when at least five of the surrounding regions contain successful retrievals.

III. MISR-MODIS Aerosol-Retrieval Comparisons

We now assess the relative performance of MISR and MODIS AOD retrievals within the MISR FOV, using the common grid points described in Section II-A to deal with spatial sampling differences. Both MISR and MODIS use different algorithmic approaches over land and water, so we make the assessments separately for the two surface categories, as much as possible. The land–water differences are most prominent in Stage 2 of the aerosol-retrieval algorithms, after acceptable retrieval regions have been selected, which occurs mainly in Stage 1, and before acceptance criteria are applied in Stage 3. A summary of how the MODIS retrieval-processing quality-assessment (QA) flags from the MODIS operational aerosol product are interpreted in this paper for classifying MODIS AOD retrieval attempts and successes, is given in Table VI. In particular, note that over water, a retrieval result is recommended for scientific use if the MODIS aerosol Estimated-Quality or Quality-Confidence (QC) flag is ≥ 1, whereas over land, only $\mathrm{QC} = 3$ are recommended for scientific use. More information about the MODIS QA and QC flags is given in [33] and [34].

Differences in instrument capabilities, along with fundamentally different assumptions about the lower boundary condition made over land and over water for each instrument, lead to coverage differences even within the MISR FOV. For example, although neither algorithm is run over totally snow- or ice-covered surfaces, the MODIS Standard over-land algorithm also does not operate over bright desert and other brighter land surfaces [23], [24]. Other sampling differences arise due to differences in cloud masking among the algorithms and, in particular, the MISR-unique angular smoothness and correlation tests.

Relative aerosol-retrieval coverage is shown in Fig. 4, which includes the latitudinal distribution of counts for successful coincident retrievals during January and July 2006 [Fig. 4(a) and (b)], as well as maps of July 2006 monthly global percent coverage for coincident MISR and MODIS observations, MISR only, and MODIS within the MISR FOV, respectively [Fig. 4(c)–(e)]. Sun glint eliminates part of the MODIS swath over dark water where off-nadir MISR cameras make aerosol retrievals possible, often leading to complementary, nonoverlapping MISR-MODIS retrieval coverage for mid- and low-latitude ocean [25]. This is shown in Fig. 4(e), where MODIS near-nadir viewing within the MISR FOV for the northern subtropical zone is almost entirely in glint. Of course, there is extensive MODIS coverage of this zone outside the MISR FOV that is not shown in these figures.

More generally, there is some coincident coverage over much of the planet on a monthly basis, and the plots reflect the distribution of factors that affect aerosol-retrieval success. The density of points varies considerably, and there is a preponderance of samples in the winter subtropics, particularly pronounced over ocean as shown in Fig. 4(a) and (b), where the MODIS glint exclusion is less severe within the MISR FOV than in the summer hemisphere. A secondary peak is shown over the summer midlatitudes in Fig. 4(a) and (b). Over land, the summer midlatitude peak is more pronounced as compared to the winter peak than for the ocean. Relatively low numbers of coincidences in the summer hemisphere near the equator are caused by the combination of glint and cloud exclusions, enhanced by the high cloud fraction associated with the intertropical convergence zone. Polar night, hemispheric differences in the land–ocean distribution, seasonal changes in snow and ice cover, and the frequency of high-latitude clouds in summer account for other attributes of the observed patterns as shown in Fig. 4(a) and (b).

Fig. 4(c)–(e) shows that the coincident sampling of MISR and MODIS [Fig. 4(c)] is dominated by the regions not excluded by the MODIS glint mask. Independently, both instruments have better sampling, even when MODIS is constrained to lie within the MISR FOV, than when the instruments are considered together. Careful inspection of Fig. 4(d) and (e) shows that MODIS has better fractional sampling over southern midlatitudes than MISR for both land and ocean situations. This may be due in part to differences in cloud screening. Resampling the data to a common resolution will not account for such differences. The full impact of differences in cloud screening on the comparative MISR and MODIS aerosol products is a topic for future work.

Kahn *et al.* [35] explored the consequences of specific MISR-MODIS algorithmic differences for AOD retrievals over ocean, based on detailed analysis of representative cases. In the next sections, we take an alternative, statistical approach for comparing the two data products. We begin by comparing MISR and MODIS AOD retrieval spatial coverage and subsequently, examine the retrieved values.

TABLE VI
QUALITY FLAG CRITERIA USED IN THIS PAPER TO ASSESS MODIS AOD RETRIEVAL ALGORITHM PERFORMANCE*

Parameter Name *(in bold italics)* and Description of Options	**Parameter Values**
Over Land	
If the Estimated-Quality (QC) flag < 3, not recommended for quantitative scientific use	
Retrieval Processing QA Flag, Part 1 (Over land, QA Part 1 applies when inversion is performed)	
Successful Retrieval (QC=3)†	0§, 5, 10
Attempt made, retrieval not recommended for quantitative scientific use includes all cases for which 0<QC<3, and some where QC=0)†	1 to 4; 6 to 9
Retrieval not attempted, see Part 2 for details (QC=0)	11
Retrieval Processing QA Flag, Part 2 (Over land, QA Part 2 applies when inversion is ***not*** performed)	
Either Part 1= any value from 0 to 10, or region not over land	0
No attempt made	1 to 6
Over Ocean	
If the Estimated-Quality (QC) flag < 1, not recommended for quantitative scientific use	
Retrieval Processing QA Flag, Part 1 (Over ocean, QA Part 1 applies when inversion is not performed)	
Either Part 2= any value from 0 to 14, or region not over ocean	0
No attempt made	1 to 10
Retrieval Processing QA Flag, Part 2 (Over ocean, QA Part 2 applies when inversion is performed)	
Successful retrieval (QC ≥ 1)†	0, 1, 3, 4, 6, 7, 8, 10, 14
Attempt made, retrieval not recommended for quantitative scientific use (QC=0)†	2, 5, 9; 11 to 13
Retrieval not attempted, see Part 1 for details (QC=0)	15

*For more detail, see Remer *et al.* [33].

†"Successful" as applied here means the AOD value is recommended for quantitative, scientific use; results designated "Attempt made, retrieval not recommended for quantitative scientific use" might still be used for qualitative mapping. The MODIS Aerosol Estimated-Quality flag, also called Quality-Confidence (QC) flag, is used to make these determinations. It has assigned values between 0 (lowest confidence) and 3. Over ocean, any QC ≥ 1 is considered successful for quantitative use. Over land, the retrieval is considered successful for quantitative use if and only if QC = 3.

§Note that over land, QA Part 1 = 0 is not sufficient for designating a result successful for quantitative scientific use.

A. MISR and MODIS AOD Retrieval Relative Coverage Statistics

Table VII gives a numerical overview of MISR, MODIS, and coincident retrieval coverage results for the area where MISR and MODIS have overlapping *InFOV* observations, stratified by over-land versus over-ocean cases. The January and July 2006 data are used for illustration. For about 8% of the total overlapping area, both algorithms attempted aerosol retrievals. This number is significantly smaller than the 14%–15% of grid points within the overall MISR FOV for which either instrument independently produced successful retrievals (Table II), primarily because of the MODIS glint and bright-surface exclusions and the MISR angular smoothness and correlation test exclusions, as discussed earlier. Over 76% of the grid points that meet both the MISR and MODIS test criteria for attempting retrievals result in successful retrievals for both instruments, amounting to about 6%–7% of coincident grid points overall.

The land–ocean stratification elaborates on these points. Between 32% and 36% of all grid points in the overlap region are considered to be over land and between 60% and 68% are over ocean. Differences between the MISR and MODIS values

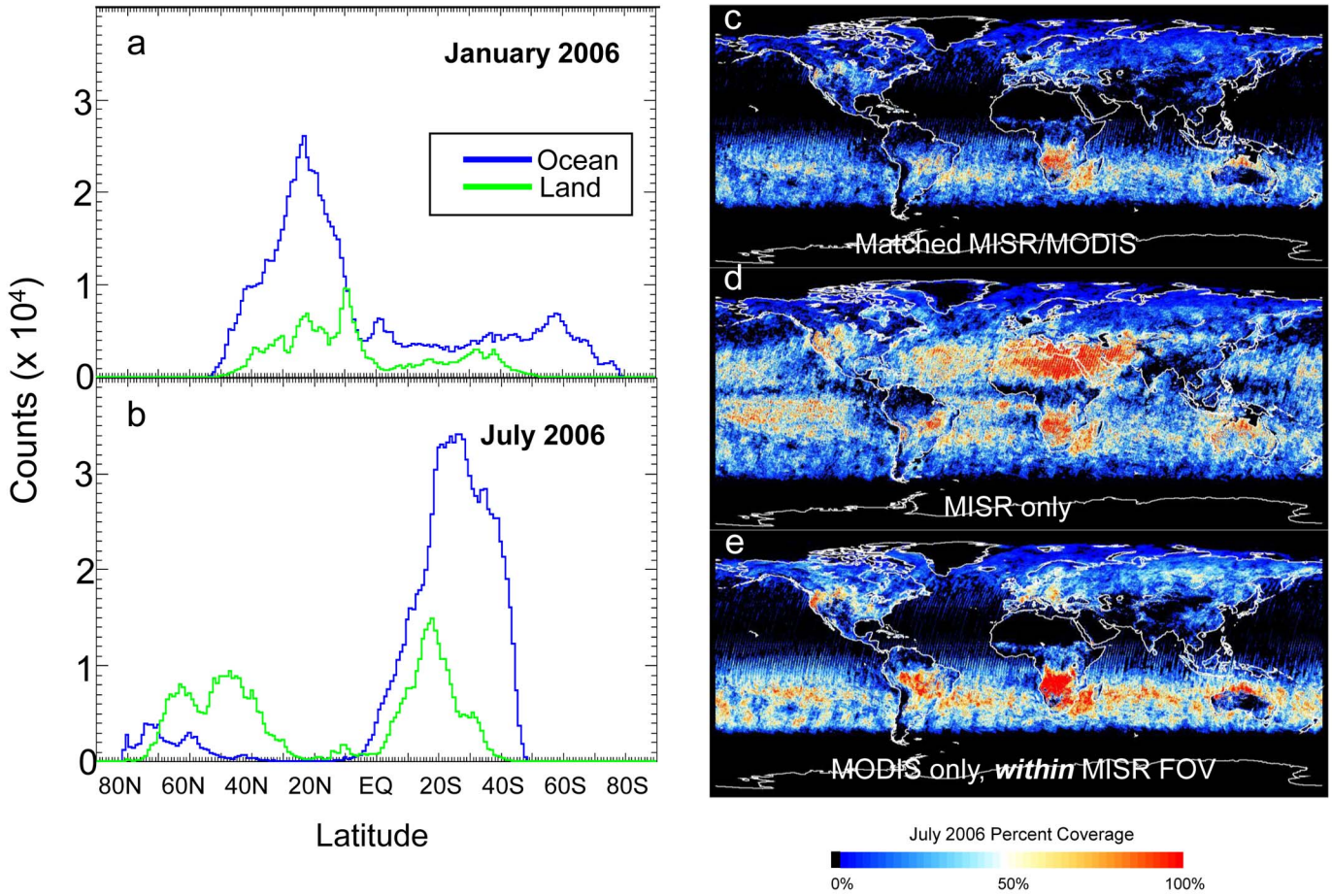

Fig. 4. Distributions of MISR and MODIS coincident retrieved AOD values over ocean and land. (a) January 2006 zonal count aggregates and (b) July 2006 zonal count aggregates. The remaining panels are July 2006 maps, showing the percent of grid points providing coverage, for (c) MISR/MODIS coincidence, (d) MISR only, and (e) MODIS only, but just within the MISR FOV.

indicate different definitions used for shallow water and coastal exclusions. Monthly differences reflect the greater landmass in the Northern Hemisphere, convolved with seasonal variations in snow cover, polar night, and cloud distribution. For example, these factors explain why a larger fraction of regions over land meet the MISR or MODIS criteria for attempting retrieval in July than in January 2006.

MISR attempted retrievals over land for 14.7% of grid points in January 2006 and over ocean for 25.4%, amounting to retrieval attempts for about 19% of all *InFOV* grid points, as listed in Table V. Because of differences between the ways "attempt" and "success" are defined in this paper (e.g., Table VI for MODIS), MODIS attempted retrievals over ocean within the MISR FOV for a smaller fraction of grid points (due primarily to glint exclusion) but reports successful results for 100% of over-ocean cases where retrievals were attempted.

Taken together, MISR and MODIS provide coincident results for about 70% of the over-land locations and between about 80% and 90% of the over-ocean locations, for situations where both algorithms attempted retrievals. This produces coincident successful retrievals for 3.4% of the total over-land coverage in January 2006. Over ocean in January and over both land and ocean in July, the corresponding values are between 7% and 8%.

B. MISR and MODIS Retrieved-AOD Comparisons

Fig. 5(a) and (b) shows scatter plots of MISR Version 22 versus MODIS/Terra Collection 5 mid-visible AOD for January 2006, contoured with a fractional power-law color scale to highlight the range of point densities, for over-ocean and over-land observations, respectively. The July 2006 results are similar, so the corresponding figures are not shown, but summary statistics for both January and July are given in Table VIII. Note that the MISR and MODIS spectral bandpasses are slightly different; for the mid-visible channels, the effective wavelengths are 557.5 and 553.7 nm, respectively. However, this difference is unlikely to significantly impact the comparisons performed in this paper [35].

The global one-month aggregates of MISR-MODIS coincident AOD retrieval values shown in Fig. 5 cover all types of conditions (see, e.g., Fig. 3), so it is not surprising that outliers occur. However, the density of points varies by over three orders of magnitude, and by far, the majority of points fall near the 1 : 1 line. *Where coincident retrievals are obtained over ocean, the correlation coefficient is about 0.9, and over land the correlation coefficient is about 0.7.* Some expected features are shown in Fig. 5, such as generally lower AOD and less scatter in the retrieved values over remote, dark, and relatively uniform ocean surfaces than land. Algorithm artifacts

TABLE VII
MISR (VERSION 22) AND TERRA/MODIS (COLLECTION 5) LAND/OCEAN AOD RETRIEVAL COVERAGE STATISTICS, FOR *Grid Points* **WITHIN THE COINCIDENT MISR AND MODIS FOV** (EXCEPT IN ROW 1, WHICH CONSIDERS ALL GRID POINTS IN THE MISR FOV), FOR JANUARY 2006 AND JULY 2006

	January 2006		**July 2006**	
Quantity	**MISR** (Approx. Percent)	**MODIS**[$] (Approx. Percent)	**MISR** (Approx. Percent)	**MODIS**[$] (Approx. Percent)
Of ***all*** grid points in the MISR FOV, percent of MISR-MODIS ***Coincident*** grid points (i.e., the actual coverage overlap)[†]	92.5		93.8	
Of MISR-MODIS coincident grid points, percent for which ***retrievals were attempted by either*** MISR or MODIS, respectively	20.4	12.1	24.1	15.4
Of MISR-MODIS coincident grid points, percent for which retrievals were ***attempted by both*** MISR and MODIS	7.3		9.2	
Of coincident grid points for which retrievals were ***attempted by either*** MISR or MODIS, respectively, percent that ***yielded either a MISR or a MODIS successful retrieval***	77.2	96.5	79.1	93.4
Of coincident grid points for which retrievals were ***attempted by both*** MISR and MODIS, percent that ***yielded both MISR and MODIS successful retrievals***	76.6		80.4	
Of ***all*** coincident grid points, percent that ***yielded both MISR and MODIS successful retrievals***	5.6		7.4	
Over Land Summaries				
Of all coincident grid points, the ***percent occurring over land***[#]	36.1	36.3	31.8	32.2
Of coincident grid points for which retrievals were ***attempted by either*** MISR or MODIS, respectively, the ***percent occurring over land***[§]	26.0	21.7	33.9	40.8
Of all coincident, over-land grid points, percent that ***yielded both MISR and MODIS successful retrievals***	3.4		7.7	
Additional Coincident, Over-Land-Only Statistics				
Grid points for which ***retrievals were attempted by either*** MISR or MODIS, respectively[§]	14.7	7.3	25.7	19.7
Grid points for which ***retrievals were attempted by both*** MISR and MODIS	4.7		11.5	
Grid points for which retrievals were ***attempted by either*** MISR or MODIS, respectively, that ***yielded either a MISR or a MODIS successful retrieval***	77.0	83.8	78.4	83.7
Grid points for which retrievals were ***attempted by both*** MISR and MODIS, ***that yielded both MISR and MODIS successful retrievals***	72.0		67.2	
Over Ocean Summaries				
Of all coincident grid points, the ***percent occurring over ocean***[#]	59.6	63.6	64.1	67.8
Of coincident grid points for which retrievals were ***attempted by either*** MISR or MODIS, respectively, the ***percent occurring over ocean***[§]	74.0	78.3	66.1	59.2
Of all coincident, over-ocean grid points, percent that ***yielded both MISR and MODIS successful retrievals***	7.3		7.7	
Additional Coincident, Over-Ocean-Only Statistics				
Grid points for which ***retrievals were attempted by either*** MISR or MODIS, respectively[§]	25.4	15.9	24.9	14.2
Grid points for which ***retrievals were attempted by both*** MISR and MODIS	9.3		8.6	
Grid points for which retrievals were ***attempted by either*** MISR or MODIS, respectively, that ***yielded either a MISR or a MODIS successful retrieval***	77.3	100.0	79.3	100.0
Grid points for which retrievals were ***attempted by both*** MISR and MODIS, that ***yielded both MISR and MODIS successful retrievals***	78.5		89.5	

[$]For MODIS, we report the "Average Retrieval" values here. The "Best Retrieval" numbers are slightly smaller.

[†]The overlap covers most of the MISR swath, but not those places where either MISR data or MODIS data are missing, mainly at the extreme north and south ends of each MISR orbit, but also individual points scattered elsewhere.

#For MISR, the percent over land and over water do not include shallow water, where retrievals are not performed.

[§]The MODIS values reported here include only those grid points within the MISR FOV, which means only near-nadir MODIS views. Sun glint preferentially eliminates near-nadir points over ocean for which MODIS attempts retrievals; this skews the fraction of attempts in favor of land. In the MODIS data set overall, about 25% of aerosol retrieval attempts are made over land, and about 75% over ocean.

are also evident, including the negative MODIS AOD values over land, which are intended to represent, in a statistical sense, retrieval uncertainty at low AOD [24]. AOD quantization noise in the MISR data appears as a positive zero-offset and subtle horizontal striping with ~0.025 AOD spacing.

A brief description of relative data-set attributes is presented next, along with an assessment of the overall MISR-MODIS relative AOD performance. However, MISR and MODIS AOD absolute accuracy and artifacts are analyzed in detail in separate publications, where direct comparisons are made with

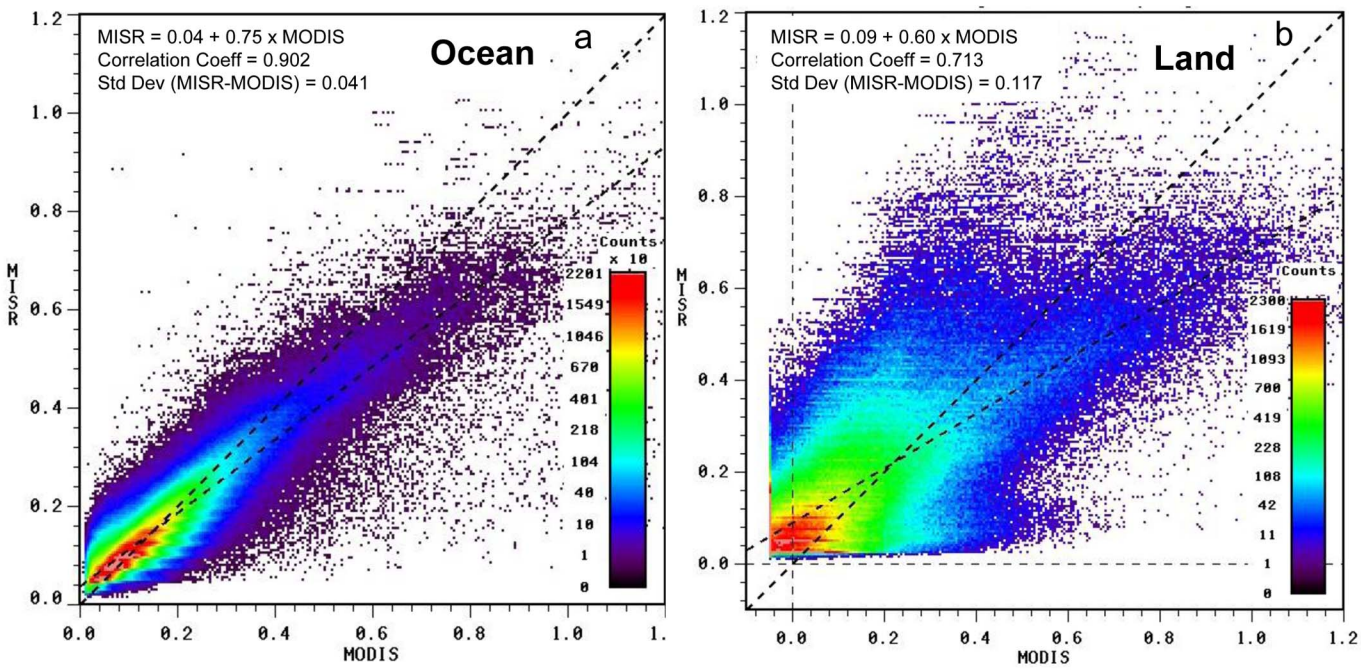

Fig. 5. Scatter plots of MISR versus MODIS coincident mid-visible AOD for January 2006, contoured using a fractional power-law color scale to show the range of point densities. (a) All over-ocean grid points. (b) All over-land grid points. For these plots, MISR Standard aerosol product Version 22 and MODIS/Terra Collection 5 data were used. The regression-line fits, correlation coefficients, and standard deviations are given in the upper left of each plot.

TABLE VIII
MISR (VERSION 22) AND TERRA/MODIS (COLLECTION 5) LAND/OCEAN COINCIDENT AOD SUMMARY STATISTICS

Data Set	Min	Max	Mean	Median	Mode	Std. Dev.	Correl. Coeff[§]	Regress. Gain[§]	Regress. Offset[§]
January 2006									
MISR Ocean	0.018	2.755	0.1404	0.122	0.1	0.0788	0.902	0.75	0.04
MODIS Ocean	0.008	4.519	0.1376	0.118	0.08	0.0974			
MISR Land	0.014	1.530	0.1618	0.117	0.05	0.1385	0.715	0.60	0.09
MODIS Land	-0.05	1.961	0.1197	0.078	-0.05 (0.00)[†]	0.1681			
July 2006									
MISR Ocean	0.014	2.794	0.1077	0.095	0.07	0.0647	0.882	0.76	0.04
MODIS Ocean	0.007	4.981	0.0941	0.077	0.04	0.0777			
MISR Land	0.014	2.208	0.1448	0.091	0.02	0.1608	0.875	0.60	0.07
MODIS Land	-0.05	4.995	0.1220	0.043	-0.05 (0.00)[†]	0.2669			

[§]The last three columns give statistics for the MISR-MODIS regression lines plotted in Figure 5. The other columns are for the individual MISR and MODIS components of the coincident data set, stratified by land and ocean.

[†]For MODIS Land, the mode is 0.0 if negative values are excluded.

quantitative surface-based Sun photometer validation data ([34] and [36], respectively, and references therein). These validation data are needed to determine the actual magnitude of retrieval errors, and they provide important clues as to the underlying causes of discrepancies.

In Fig. 5, the MISR AOD distributions are skewed to lower values than MODIS over both ocean and land, and the slopes of the regression lines are correspondingly less than unity (0.75 over ocean and 0.60 over land). However, taken over the entire data set, MISR mean AOD values are *higher* than MODIS over

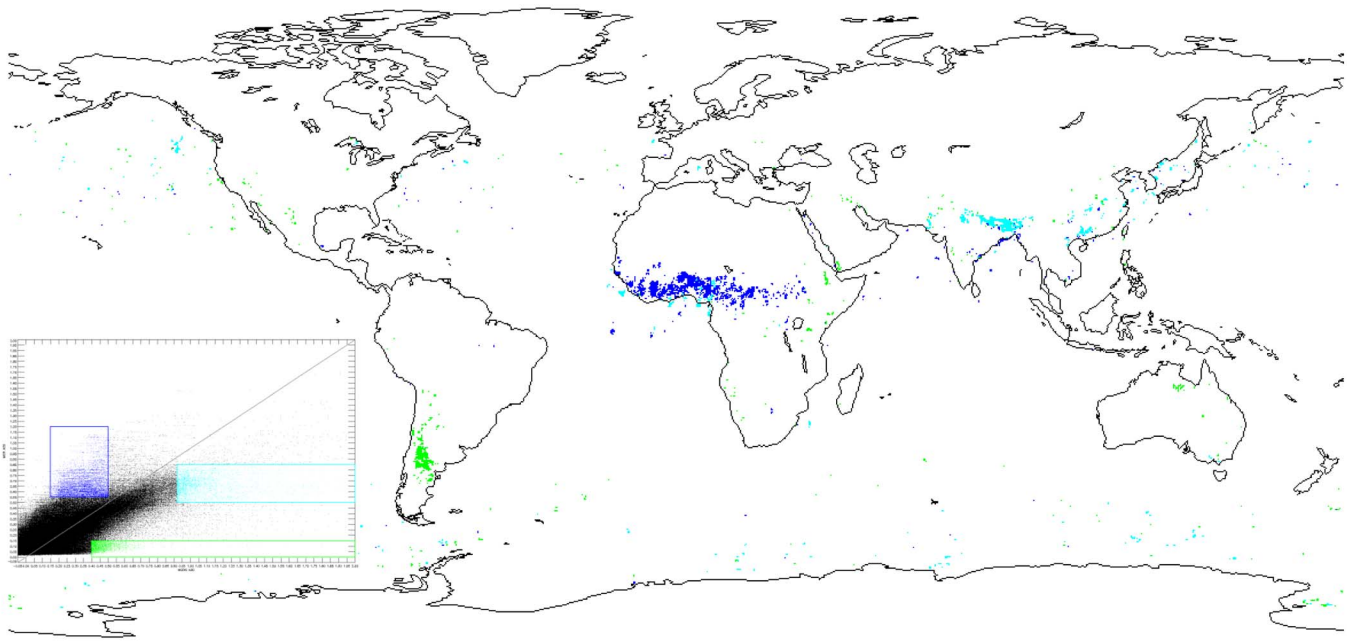

Fig. 6. Geographical distribution of point clusters in the scatter plot of MISR versus MODIS coincident mid-visible AOD for January 2006. The point cluster where MISR AOD is significantly higher than MODIS is shown in dark blue. The high-AOD point cluster for both MISR and MODIS, with MODIS higher than MISR, is colored cyan. The point cluster where MODIS AOD is significantly higher than MISR is highlighted in green.

both ocean and land (Table VIII). Careful examination of Fig. 5 reveals that, for low AOD, MISR values are higher than MODIS over both ocean and land, whereas for AOD greater than about 0.2 or 0.3, MISR AODs are systematically lower than MODIS. The low-AOD regime dominates the average statistics due to the density of points, and the high-AOD cases leverage the regression line fits, but both regimes are evident in the plots. Over water, the gap in MISR low-AOD values between zero and about 0.02 contributes to the higher MISR average AOD, although this might not be the sole factor involved. Over land, the negative AOD values introduced in MODIS Collection 5 contribute to the MISR-MODIS low-AOD discrepancy. This MODIS Collection 5 algorithm change reversed a condition that applied to previous MODIS aerosol product versions, where MODIS AOD values were substantially higher than MISR and AERONET over land for small AOD as well as large [2], [7].

In the high AOD regime, MISR Version 22 is known to underestimate AOD in some circumstances, such as when aerosols are present having smaller single-scattering albedo (SSA) than those included in the retrieval algorithm climatology, and frequently over land when AOD exceeds about 0.6; these issues are discussed in detail elsewhere [6], [14], [36].

The distribution of values shown in Fig. 5(b) also suggests that, at least in the over-land data, there are several distinct groupings of points that the MISR and MODIS algorithms treat qualitatively differently. Most of these points, colored dark blue and purple in the figure, represent very small fractions of the global collection of coincident retrievals. To better understand these differences, Fig. 6 shows the geographic locations corresponding to some of these groupings in the January 2006 coincident land–ocean distribution. In this figure, dark blue isolates the geographic locations of the point cluster for which MISR values exceed those of MODIS by a factor around 1.7. This cluster comes almost exclusively from an over-land band across North–Central Africa, a region where mixtures of biomass burning smoke and desert dust particles are prevalent. A lack of this aerosol mixture category in the MISR aerosol-retrieval algorithm climatology for all versions up to 22 has been highlighted based on discrepancies with coincident AERONET AOD observations and validated with MISR research aerosol-retrieval analyses [6], [14], [36]. Although the MODIS algorithm is designed to find solutions that mix coarse-mode dust with fine-mode smoke in that region, errors may be large as well, due to relatively bright surfaces and uncertainties in the assumed aerosol properties. Upgrades to the MISR algorithm are under consideration, making use of the spherical versus nonspherical particle discrimination possible with this instrument to help identify such smoke–dust mixtures.

Cyan in Fig. 6 isolates geographically the cluster of high AOD points for both MISR and MODIS. This group is localized primarily over land at the eastern end of the Indo–Gangetic plain in northern India and Bangladesh, where AOD is high and particle SSA is often low, particularly during northern winter [3]. These conditions exacerbate the high-AOD issues discussed in relation to Fig. 5.

A third cluster shown in Fig. 5(b), for which MODIS values are larger than MISR, having a slope of about 0.25, represents a very small number of points coming primarily from the Patagonia Desert region of South America [37], with an additional cluster of points in North–Central Australia in the vicinity of the Georgina Basin and the Barkly Tableland (green in Fig. 6). These regions are extremely arid, and vegetation is sparse. As the MODIS land algorithm has difficulty retrieving aerosols over bright surfaces, most of the significant desert

regions of the world are excluded [e.g., Fig. 4(e)]. However, MODIS bright-surface screening seems to miss these smaller arid regions, resulting in unduly high MODIS AOD retrievals. Interestingly, the corresponding point cluster is nearly absent from the July 2006 data (not shown), which is during the wet season, when a somewhat darker, more vegetated surface would be expected.

In summary, the correlation between MISR and MODIS AOD for matched retrievals over the entire globe for a full month comes to about 0.9 and 0.7 over ocean and land, respectively. Specific differences identified with clusters of points are traced to algorithm issues that have been documented elsewhere in the context of quantitative validation data from suborbital measurements, although this does not preclude the possibility of other mechanisms contributing to aerosol-retrieval error. Algorithm upgrades are planned for the better-constrained and more tractable situations.

C. MISR and MODIS Retrieved-AOD Difference Envelopes

We now assess statistically the differences between coincident MISR and MODIS retrieved AOD values. Based on comparisons between MISR early postlaunch (Version 12) aerosol-retrieval results and two years of coincident AERONET Sun photometer observations, Kahn *et al.* [6] concluded that about two-thirds of MISR mid-visible AOD values fell within ± 0.05 or $0.2 \times$ AOD of the corresponding validation value, whichever is larger, and more than a third met the more stringent criterion ± 0.03 or $0.1 \times$ AOD. The sampling included a broad range of aerosol air mass types as well as surface types, and stratification revealed patterns within this overall result.

The combination of a relative (e.g., 20% or 10% of AOD) and an absolute (e.g., 0.05 or 0.03) condition is required to assess AOD agreement over the full range of retrieved values. At high AOD, the relative condition captures variability and uncertainty that scale with AOD itself, whereas for low AOD, the absolute condition accounts for retrieval errors that do not disappear as AOD approaches zero. The relative condition dominates when $\mathrm{AOD} > 0.25$ and $\mathrm{AOD} > 0.3$ for the looser and more stringent MISR agreement criteria, respectively. In addition, as pointed out in Kahn *et al.* [6], the impact of the MISR cloud screening process was not tested in that study, because coincident data are obtained only when both the MISR and AERONET algorithms determine that a scene is cloud free.

In a comprehensive comparison study between MODIS early postlaunch AOD and coincident AERONET data, Remer *et al.* [23] concluded that 67% of MODIS values fell within $\pm 0.03 \pm 0.05 \times$ AOD of the ground-truth values over ocean and within $\pm 0.05 \pm 0.15 \times$ AOD over land. (The notation used here indicates, for example, that relative to AERONET, 67% of MODIS AOD values over ocean fell within an envelope defined by an absolute uncertainty of 0.03, aggregated with a relative uncertainty of 5% of the AOD value itself.) One difference between the MISR and MODIS validation analyses is that the MODIS over-land statistics did not include desert or other bright-surface retrievals, which produced the lowest correlations of all the aerosol-type categories aggregated in the overall MISR validation result [6].

MISR-MODIS AOD comparisons differ fundamentally from the MISR-AERONET and MODIS-AERONET comparisons described earlier. AERONET direct-Sun measurements represent independently cloud-screened ground truth, whereas MISR and MODIS scattered-light retrievals each entail larger uncertainties and as such, cannot be used to validate the AOD absolute accuracy of either instrument. Nevertheless, we can test the consistency of the two satellite data sets, with the understanding that if, for a given AOD regime, one satellite data set is systematically higher than ground truth and the other is systematically lower, the validation criteria summarized earlier could be met even if the MISR-MODIS AOD spread is larger than the results obtained in either of the individual AERONET-based validation studies.

The following equations parallel the envelopes derived in the MISR-AERONET validation study [6]:

$$|\mathrm{AOD}_{\mathrm{MISR}} - \mathrm{AOD}_{\mathrm{MODIS}}| \leq \max[0.05, 0.2 \times \mathrm{AOD}_{\mathrm{MODIS}}] \tag{1}$$

$$|\mathrm{AOD}_{\mathrm{MISR}} - \mathrm{AOD}_{\mathrm{MODIS}}| \leq \max[0.03, 0.1 \times \mathrm{AOD}_{\mathrm{MODIS}}] \tag{2}$$

where a MISR-MODIS-coincident AOD pair satisfying (1) would meet the looser criterion and an AOD pair satisfying (2) would meet the more stringent criterion. As neither MISR nor MODIS represents ground truth, we arbitrarily placed the MODIS AOD on the right-hand side of these equations as "truth," ignoring for the moment the additional uncertainty represented by the MODIS AOD validation envelope. Table IX displays the results for the total data set, and stratified by ocean and land, for January and July 2006. In both months, the overall MISR-MODIS AOD spread falls within the validation envelope determined by the MISR-AERONET AOD comparison. However, this result is dominated by the over-ocean values, which, for the MISR Version 22 and MODIS Collection 5 data, are in significantly closer agreement than the validation envelope established with the MISR Version 12 data.

Despite the narrow spread between the MISR and MODIS over-ocean AOD values, only about a third of the over-land data meet criterion (1) and less than a fifth qualifies based on (2) (Table IX). To test whether the over-land values meet the *actual* criteria obtained from the AERONET validation studies, however, we must allow for the envelope associated with MODIS as well as MISR, because the differences between each instrument's retrieved values and ground truth are not randomly distributed within their respective sensitivity envelopes. For a large fraction of cases, when one instrument is at the high end of its sensitivity envelope relative to ground truth, the other is at the low end due to specific assumptions made in the algorithms [35]. We take the approach of concatenating the two sensitivity envelopes, as our purpose here is to test for minimal consistency with previously published studies. Formal validation is accomplished by directly comparing the data from each instrument with ground truth, as this eliminates the key ambiguity about the distribution of points within each envelope.

If the MODIS value $(\mathrm{AOD}_{\mathrm{MODIS}})$ for an over-land case is at the low-end limit of the MODIS one $-\sigma$ envelope [23] relative

TABLE IX
PERCENT OF MISR-MODIS COINCIDENT AOD PAIRS MEETING THE LOOSER AND MORE STRINGENT CRITERIA REPRESENTED BY EQUATIONS (1) AND (2) AND EQUATIONS (4) AND (5)†

	January			July		
	Total	**Ocean**	**Land**	**Total**	**Ocean**	**Land**
Eq. 1 (MISR, loose)	73.6	85.3	31.8	70.2	88.4	33.5
Eq. 2 (MISR, stringent)	53.8	63.8	18.1	51.1	67.4	18.3
Eq. 4a & 4b† (Combined, loose)	90.1	95.7	69.9	91.8	96.8	81.7
Eq. 5a & 5b† **(Combined, stringent)**	84.1	91.1	59.2	84.6	93.3	67.0

†For the over-ocean values reported here, Equations (4) and (5) were modified to reflect the MODIS over-ocean validation envelope ($\pm 0.03 \pm 0.05 \times$ AOD), rather than the less stringent over-land envelope.

to the true optical depth (AOD^-), the two values are related as

$$\mathrm{AOD}_{\mathrm{MODIS}} = \mathrm{AOD}^- - 0.15 \times \mathrm{AOD}^- - 0.05. \quad (3a)$$

Similarly, if $\mathrm{AOD}_{\mathrm{MODIS}}$ is at the high-end limit, the true optical depth (AOD^+) is related as

$$\mathrm{AOD}_{\mathrm{MODIS}} = 1.15 \times \mathrm{AOD}^+ + 0.05. \quad (3b)$$

For a given over-land $\mathrm{AOD}_{\mathrm{MODIS}}$ within the one $-\sigma$ envelope, the true optical depth can fall anywhere between AOD^- and AOD^+. If the corresponding MISR AOD value $(\mathrm{AOD}_{\mathrm{MISR}})$ is larger than $\mathrm{AOD}_{\mathrm{MODIS}}$, the relationship between the largest possible $\mathrm{AOD}_{\mathrm{MISR}}$ within the MISR envelope $(\max[(\mathrm{AOD} + 0.05; 1.2 \times \mathrm{AOD}])$ [6] and the smallest $\mathrm{AOD}_{\mathrm{MODIS}}$ value within the MODIS over-land envelope is

$$\mathrm{AOD}_{\mathrm{MISR}} \leq \max\left\{\left[\frac{(\mathrm{AOD}_{\mathrm{MODIS}} + 0.05)}{0.85} + 0.05\right]; \left[1.2 \times \frac{(\mathrm{AOD}_{\mathrm{MODIS}} + 0.05)}{0.85}\right]\right\} \quad (4a)$$

where we solved (3a) for AOD^- to provide a true AOD limit for the low MODIS case. Conversely, when $\mathrm{AOD}_{\mathrm{MODIS}} > \mathrm{AOD}_{\mathrm{MISR}}$, this time using AOD^+ from (3b), the combined envelope limit is

$$\mathrm{AOD}_{\mathrm{MISR}} \geq \min\left\{\left[\frac{(\mathrm{AOD}_{\mathrm{MODIS}} - 0.05)}{1.15} - 0.05\right]; \left[0.8 \times \frac{(\mathrm{AOD}_{\mathrm{MODIS}} - 0.05)}{1.15}\right]\right\}. \quad (4b)$$

Therefore, for consistency with the previous MISR and MODIS independent validation results against AERONET, one would expect at least the conditions of (4a) and (4b) to be met by the MISR-MODIS direct comparison performed in this paper. The values are given in Table IX, and even over land, they meet this criterion; well over two-thirds of the over-land data fall within the combined envelope. Recasting (4a) and (4b) using the more stringent MISR condition $(\max[(\mathrm{AOD} + 0.03; 1.1 \times \mathrm{AOD}])$, we have

$$\mathrm{AOD}_{\mathrm{MISR}} \leq \max\left\{\left[\frac{(\mathrm{AOD}_{\mathrm{MODIS}} + 0.05)}{0.85} + 0.03\right]; \left[1.1 \times \frac{(\mathrm{AOD}_{\mathrm{MODIS}} + 0.05)}{0.85}\right]\right\} \quad (5a)$$

$$\mathrm{AOD}_{\mathrm{MISR}} \geq \min\left\{\left[\frac{(\mathrm{AOD}_{\mathrm{MODIS}} - 0.05)}{1.15} - 0.03\right]; \left[0.9 \times \frac{(\mathrm{AOD}_{\mathrm{MODIS}} - 0.05)}{1.15}\right]\right\}. \quad (5b)$$

The results, also given in Table IX, again represent substantially closer agreement than minimally required for consistency with the published MISR and MODIS validation-study conclusions. However, this agreement in itself does not speak to the quality of the products overall, which is covered in Section III-B and references therein, particularly those studies involving comparisons with ground-truth validation data.

D. MISR-MODIS ANG-Retrieval Comparisons

Over ocean, both MISR and MODIS retrieve values of the Angstrom exponent (ANG). ANG is defined as the negative slope of the least square line, fit to the logarithm of spectral AOD versus logarithm of wavelength plot. It is a single variable related to the particle size for monomodal aerosol distributions. For MISR, this quantity is evaluated based on a least squares fit to the AOD in the four spectral bands; for MODIS, AOD at two limiting wavelengths are used. MODIS retrieves ANG over ocean; the MODIS over-land ANG is considered an algorithm diagnostic and is primarily assumed, based on location and seasonal considerations [23], [24]. To compare over-ocean MODIS and MISR ANG, we adopt the MODIS Angstrom_Exponent_1_Ocean product, assessed from the retrieved 0.55- and 0.86-μm AOD. The results are shown in the contoured scatter plots of Fig. 7.

When all available data are considered [Fig. 7(a)], the correlation between the MISR and MODIS ANG is 0.44, showing, at least, consistency in distinguishing air masses dominated by fine-mode from coarse-mode particles. However, as indicated in the MISR data-quality statement and references therein, when $\mathrm{AOD}_{\mathrm{MISR}}$ is below about 0.15 or 0.2, there is less information about aerosol microphysical properties in the observed radiances. Although the AOD retrieval is robust in this AOD regime, many different aerosol mixtures can meet the MISR algorithm acceptance criteria, and ANG, calculated from an average of the AOD values obtained in each MISR spectral channel, tends toward unity. At low AOD, MODIS sensitivity to particle microphysical properties is also diminished. Fig. 7(b) shows MISR-MODIS coincident ANG values only for points having MISR-retrieved mid-visible AOD > 0.2. In this case, the correlation coefficient rises to 0.67.

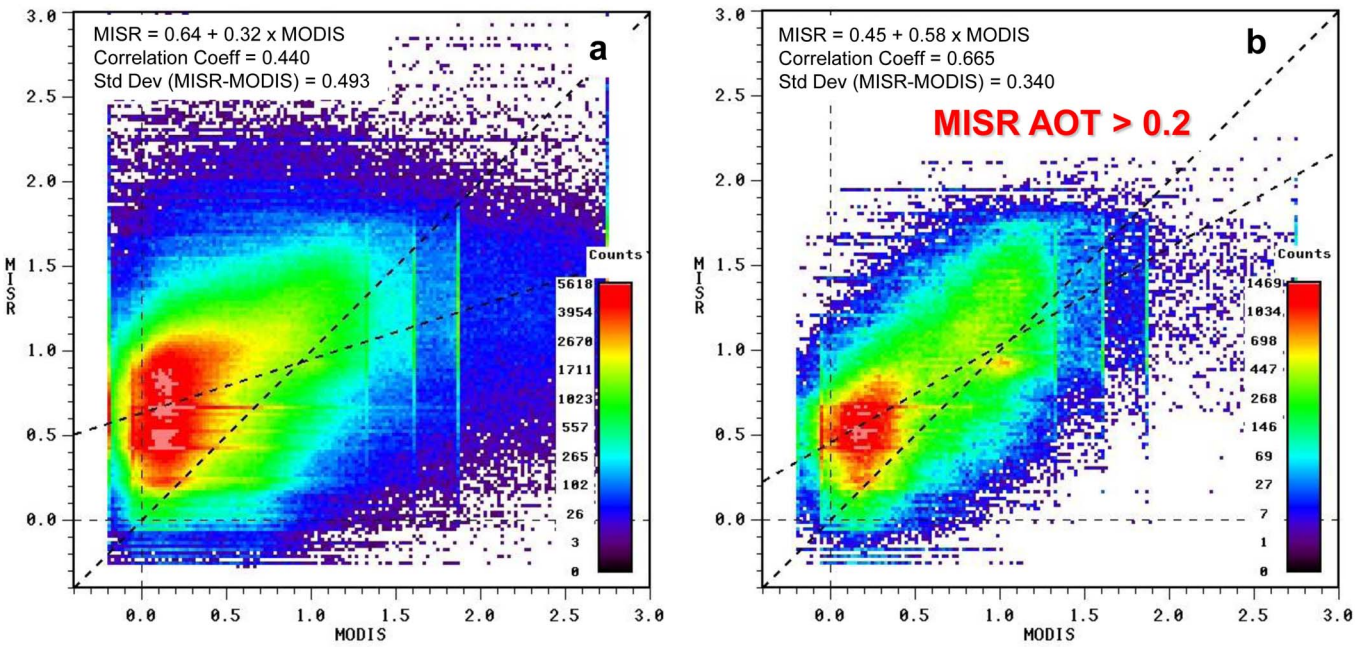

Fig. 7. Scatter plots of MISR (Version 22) versus MODIS/Terra (Collection 5) over-ocean ANGs for January 2006, contoured using a fractional power-law color scale to show the range of point densities. The MODIS Angstrom_Exponent_1_Ocean product, assessed from the retrieved 0.55- and 0.86-μm MODIS AOD values is presented. (a) All over-ocean points in the MISR-MODIS coincident data set. (b) Only points for which MISR mid-visible AOD > 0.2, i.e., only those points which meet the minimum AOD validation criterion for MISR aerosol property retrievals. The regression-line fits, correlation coefficients, and standard deviations are given in the upper left of the plots.

IV. Summary and Conclusion

This paper reviews MISR aerosol-retrieval quality flags and coverage statistics, using the Version 22 product for January and July 2006 as a representative example. It also describes MISR-MODIS coincident aerosol-retrieval coverage and offers a statistical assessment of the relative MISR Version 22 and MODIS/Terra Collection 5 AOD retrieval performance, for all locations where both algorithms report values. Remaining algorithm issues are highlighted as appropriate, but detailed validation is provided in other papers that incorporate ground-truth validation data essential to quantitatively assessing the satellite remote sensing results.

Globally, MISR and MODIS each obtain successful aerosol retrievals for *InFOV* grid points about 15% of the time. About 43% of locations are eliminated explicitly due to cloud screening; other locations are excluded due primarily to low Sun angles at high latitudes and polar night, complex terrain, glint, or a combination of factors. This result in part reflects compromises that must be made between coverage and data quality, particularly for algorithms that must run efficiently on immensely diverse global data sets. The high-spatial-resolution (250–275 m/pixel) imaging data from both instruments, along with an assumption about aerosol distribution uniformity on $\sim$10-km spatial scales, make it possible to avoid most clouds and other obstacles, significantly increasing coverage relative to what would be possible with only coarser-resolution data.

Coincident MISR-MODIS aerosol retrievals are obtained for about 6%–7% of the total overlap region, amounting to about half the locations where each instrument individually produces successful retrievals. Other potential coincident retrievals are eliminated due primarily to MODIS glint and bright land-surface exclusions and MISR angular smoothness and correlation masking. For both MISR and MODIS, successful retrievals are obtained for over 75% of the locations where attempts are made. The general behavior of these aspects of the MISR algorithm decision-making process can be mapped out using the aerosol product quality indicators (e.g., Fig. 3).

Where MISR-MODIS coincident AOD retrievals are obtained over ocean, the correlation coefficient is about 0.9, and over land, the correlation coefficient is about 0.7. Agreement between the two sets of retrieval results is well within previously published validation envelopes for both ocean and land. In making such comparisons, the convolution of these envelopes must be taken into account, as one instrument's retrieved value may be skewed high relative to ground truth when the other instrument value is skewed low. That this is the case for a large fraction of the MISR-MODIS coincident cases indicates that much of the remaining error is not random. This, in turn, suggests that some refinement of the algorithms may be possible, based on correcting known issues [6], [14], [16]. However, "fixing" the algorithms is more challenging than identifying and understanding the issues, as these algorithms must handle all situations that arise, for the entire global data set, efficiently and automatically.

The over-ocean ANG comparisons yield a correlation of 0.67 when points for which $\mathrm{AOD_{MISR}} > 0.2$ are considered, as required for well-constrained particle microphysical property retrievals according to the MISR aerosol product quality statement. Accordingly, the over-ocean ANGs for both instruments are generally consistent in distinguishing aerosol air masses dominated by coarse-mode versus fine-mode particles.

In a recent paper, Liu and Mishchenko [38] reached a number of conclusions that are contradicted by the results presented in this paper. The differences can be traced to misinterpretation of the satellite data sets that the current paper aims to clarify for the benefit of future users.

1) Liu and Mishchenko [38] report "essentially no correlation" between the MISR and MODIS ANGs. Their approach was to generate scatter plots from the monthly global coincidences for January 2006, without accounting for the density of points [38, Fig. 3]. Their paper does not report a correlation coefficient or related quantitative summary statistic. The actual point density varies by more than three orders of magnitude (Fig. 7 of the current paper). Given the diversity of conditions over the globe, as illustrated in Section II-B, some outliers are to be expected. However, these are overemphasized in the Liu and Mishchenko plot, which effectively weights isolated outliers more heavily than the densely overplotted concentration of points near the 1 : 1 line. In generating their ANG plots, Liu and Mishchenko [38] also include low-AOD points. The MISR aerosol product data-quality statement cautions that the satellite data have limited sensitivity to particle microphysical properties when the retrieved mid-visible AOD is below 0.15 or 0.2. Furthermore, they present MISR versus MODIS/Terra ANG over land. The MODIS algorithm over land has limited information content. The reported MODIS ANG is considered an algorithm diagnostic, so the unnatural clustering of points in their figure reflects primarily the algorithm assumptions rather than a retrieved result [23], [33]. MISR ANG over land has been validated by comparisons with coincident AERONET Sun photometer measurements [6], [36].
2) Liu and Mishchenko [38] provide similar scatter plots for their MISR-MODIS AOD comparisons, and over land, they conclude that: "agreement is poor or even unacceptable." Again, the representation of outliers is exaggerated because the two-to-three orders-of-magnitude variation in point density is not taken into account (compare [38, Fig. 1] with Fig. 5 of the current paper). Over land, only MODIS AOD values for which the Estimated Quality (QC) flag equals three are recommended for scientific use (e.g., Table VI), a suggestion not followed by Liu and Mishchenko [38]. In addition, the actual MISR and MODIS AOD results are far better understood than these authors suggest. As discussed earlier, accounting for differences in low- and high-AOD algorithm behavior is key to understanding retrieval performance. Moreover, in Fig. 6, the main clusters of outliers in the MISR-MODIS AOD comparison plots are traced to specific geographic regions where known algorithm issues arise, such as locations with mixtures of biomass burning and dust aerosols that are not accounted for in the current algorithm version particle climatologies (detailed analysis of these issues is provided in the references cited in Section III-B).
3) Liu and Mishchenko [38] also state the following: "... the identified differences between the MODIS and MISR Level 2 [AOD] results often significantly exceed the respective accuracy claims..." published by Kahn *et al.* [6] and Remer *et al.* [23]. This conclusion is based on an analysis of MISR-MODIS coincidence statistics in which one satellite AOD product is treated as ground truth, rather than by convolving the reported validation envelopes of the two instruments. As presented in Section III-C, when the validation envelopes are convolved appropriately, the coincident MODIS Collection 5 and MISR Version 22 AODs are in closer agreement than the published results derived from the early postlaunch products.

The analysis presented in this paper confirms MISR and MODIS aerosol-retrieval performance as reported by the instrument teams and many others in previous work and adds considerable detail to some aspects of the published MISR product descriptions. Both the strengths and limitations of the products are revealed by these studies. For example, the aerosol data have inherent clear-sky and time-of-day biases, and there is a high-AOD bias to the retrieved particle microphysical properties, as sensitivity to particle properties is diminished at low AOD. And there can be significant AOD variability on spatial scales well below the standard product resolution, especially in aerosol source regions and near clouds. Other issues identified in this paper and in previous work [6], [14], [16], [24], [35], [36], [39] relate to cloud contamination and algorithm assumptions that are not valid under certain circumstances, some of which can be resolved in future versions of the retrieval algorithms.

Due to sampling limitations and other factors, MISR and MODIS representations of aerosol amount and type must be used with care when assessing monthly global direct aerosol radiative forcing (DARF) and AOD trends. Specifically, actual satellite sampling must be evaluated in light of aerosol field variability, on the spatial and temporal scales of interest. Major advances in large-scale and long-term trend studies will likely require combining three elements: 1) spatially extensive satellite-derived maps of AOD and aerosol air mass type, curtains of AOD vertical distribution from space-based lidar, near-source aerosol plume-height maps from stereo imaging, and possibly high-temporal-resolution AOD or aerosol index from geostationary imaging; 2) *in situ* sampling, providing SSA, aerosol chemistry, etc., to fill in the needed microphysical detail that is specific to each aerosol air mass type, at a level of accuracy unobtainable from space; 3) ground truth to validate the more extensive satellite aerosol products. The resulting, spatially extensive snapshots will then be used to constrain aerosol transport models, which in turn will effectively interpolate in space and time, providing DARF, anthropogenic component of DARF, and material fluxes. Even so, the MISR, as well as the MODIS products, can be and have been used directly for many applications, such as regional AOD gradient and aerosol air mass type mapping, aerosol source plume-injection-height characterization, real-time air-quality monitoring, long-term aerosol-pollution exposure, qualitative hemispheric-to-global-scale long-term trends, and aerosol transport model validation.

We continue to learn about the information content of the MISR multispectral multiangle radiance observations from comparisons with field campaign and surface network data, and from the growing range of studies to which the data are being applied. These insights can help us further refine the

aerosol-retrieval algorithms and provide yet more complete characterization of the results. The experience, along with the results, should also prove useful in planning future missions aimed at further reducing the uncertainties in aerosol impacts on the environment.

ACKNOWLEDGMENT

The authors would like to thank their colleagues at the NASA Langley Research Center's Atmospheric Sciences Data Center for their roles in producing the MISR data sets; L. Di Girolamo, J. Pierce, D. Wu, and several anonymous reviewers for helpful comments on early versions of this paper; D. McDonald, T. Nolan, and B. Rheingans for contributions to Fig. 1; and C. Newman for helping prepare this paper. This work was performed in part at the NASA Goddard Space Flight Center and in part at the Jet Propulsion Laboratory, California Institute of Technology, under a contract with NASA.

REFERENCES

[1] J. V. Martonchik, R. A. Kahn, and D. J. Diner, "Retrieval of aerosol properties over land using MISR observations," in *Satellite Aerosol Remote Sensing Over Land*, A. Kokhanovsky, Ed. Berlin, Germany: Springer-Verlag, 2009.

[2] W. A. Abdou, D. J. Diner, J. V. Martonchik, C. J. Bruegge, R. A. Kahn, B. J. Gaitley, K. A. Crean, L. A. Remer, and B. Holben, "Comparison of coincident MISR and MODIS aerosol optical depths over land and ocean scenes containing AERONET sites," *J. Geophys. Res.*, vol. 110, p. D10 S07, 2005. DOI:10.1029/2004JD004693.

[3] L. Di Girolamo, T. C. Bond, D. Bramer, D. J. Diner, F. Fettinger, R. A. Kahn, J. V. Martonchik, M. V. Ramana, V. Ramanathan, and P. J. Rasch, "Analysis of multi-angle imaging spectroradiometer (MISR) aerosol optical depths over greater India during winter 2001–2004," *Geophys. Res. Lett.*, vol. 31, no. 23, p. L23 115, 2004. DOI:10.1029/2004GL021273.

[4] D. J. Diner, B. H. Braswell, R. Davies, N. Gobron, J. Hu, Y. Jin, R. A. Kahn, Y. Knyazikhin, N. Loeb, J.-P. Muller, A. W. Nolin, B. Pinty, C. B. Schaaf, G. Seiz, and J. Stroeve, "The value of multi-angle measurements for retrieving structurally and radiatively consistent properties of clouds, aerosols, and surfaces," *Remote Sens. Environ.*, vol. 97, no. 4, pp. 495–518, Sep. 2005.

[5] X. Jiang, Y. Liu, B. Yu, and M. Jiang, "Comparison of MISR aerosol optical thickness with AERONET measurements in Beijing metropolitan area," *Remote Sens. Environ.*, vol. 107, no. 1/2, pp. 45–53, Mar. 2007.

[6] R. Kahn, B. Gaitley, J. Martonchik, D. Diner, K. Crean, and B. Holben, "MISR global aerosol optical depth validation based on two years of coincident AERONET observations," *J. Geophys. Res.*, vol. 110, no. D10, p. D10 S04, 2005. DOI:10:1029/2004JD004706.

[7] S. Kinne, M. Schulz, C. Textor, S. Guibert, Y. Balkanski, S. E. Bauer, T. Berntsen, T. F. Berglen, O. Boucher, M. Chin, W. Collins, F. Dentener, T. Diehl, R. Easter, J. Feichter, D. Fillmore, S. Ghan, P. Ginoux, S. Gong, A. Grini, J. Hendricks, M. Herzog, L. Horowitz, I. Isaksen, T. Iversen, A. Kirkevåg, S. Kloster, D. Koch, J. E. Kristjansson, M. Krol, A. Lauer, J. F. Lamarque, G. Lesins, X. Liu, U. Lohmann, V. Montanaro, G. Myhre, J. E. Penner, G. Pitari, S. Reddy, O. Seland, P. Stier, T. Takemura, and X. Tie, "An AeroCom initial assessment—Optical properties in aerosol component modules of global models," *Atmos. Chem. Phys.*, vol. 6, pp. 1815–1834, 2006.

[8] Y. Liu, J. A. Sarnat, B. A. Coull, P. Koutrakis, and D. J. Jacob, "Validation of MISR aerosol optical thickness measurements using Aerosol Robotic Network (AERONET) observations over the continuous United States," *J. Geophys. Res.*, vol. 109, p. D06 205, 2004. DOI:10.1029/2003JD003981.

[9] J. V. Martonchik, D. J. Diner, R. A. Kahn, B. J. Gaitley, and B. N. Holben, "Comparison of MISR and AERONET aerosol optical depths over desert sites," *Geophys. Res. Lett.*, vol. 31, no. 16, p. L16 102, 2004. DOI:10.1029/2004GL019807.

[10] G. Myhre, T. F. Berglen, C. R. Hoyle, S. A. Christopher, H. Coe, J. Crosier, P. Formenti, J. M. Haywood, M. Johnsrud, T. A. Jones, N. Loeb, S. Osborne, and L. A. Remer, "Modeling of chemical and physical aerosol properties during the ADRIEX aerosol campaign," *Q.J.R. Meteorol. Soc.*, vol. 135, no. 638, pp. 53–66, Jan. 2009.

[11] J. Redemann, B. Schmid, J. A. Eilers, R. Kahn, R. C. Levy, P. B. Russell, J. M. Livingston, P. V. Hobbs, W. L. Smith, Jr., and B. N. Holben, "Suborbital measurements of spectral aerosol optical depth and its variability at sub-satellite-grid scales in support of CLAMS, 2001," *J. Atmos. Sci.*, vol. 62, no. 4, pp. 993–1007, Apr. 2005.

[12] D. R. Reidmiller, P. V. Hobbs, and R. Kahn, "Aerosol optical properties and particle size distributions on the east coast of the United States, derived from airborne *in situ* and remote sensing measurements," *J. Atmos. Sci.*, vol. 63, no. 3, pp. 785–814, Mar. 2006.

[13] B. Schmid, J. Redemann, P. B. Russell, P. V. Hobbs, D. L. Hlavka, M. J. McGill, B. N. Holben, E. J. Welton, J. R. Campbell, O. Torres, R. A. Kahn, D. J. Diner, M. C. Helmlinger, D. A. Chu, C. Robles Gonzalez, and G. de Leeuw, "Coordinated airborne, spaceborne, and ground-based measurements of massive, thick aerosol layers during the dry season in southern Africa," *J. Geophys. Res.*, vol. 108, no. D13, p. 8496, 2003. DOI:10.1029/2002JD002297.

[14] W.-T. Chen, R. Kahn, D. Nelson, K. Yau, and J. Seinfeld, "Sensitivity of multi-angle imaging to optical and microphysical properties of biomass burning aerosols," *J. Geophys. Res.*, vol. 113, p. D10 203, 2008. DOI:10.1029/2007JD009414.

[15] R. Kahn, A. Petzold, M. Wendisch, E. Bierwirth, T. Dinter, M. Esselborn, M. Fiebig, B. Heese, P. Knippertz, D. Muller, A. Schladitz, and W. von Hoyningen-Huene, "Desert dust aerosol air mass mapping in the western Sahara, using particle properties derived from space-based multi-angle imaging," *Tellus*, vol. 61, no. 1, pp. 239–251, 2008.

[16] R. Kahn, Y. Chen, D. L. Nelson, F.-Y. Leung, Q. Li, D. J. Diner, and J. A. Logan, "Wildfire smoke injection heights—Two perspectives from space," *Geophys. Res. Lett.*, vol. 35, no. 4, p. L04 809, Feb. 2008. DOI:10.1029/2007GL032165.

[17] Y. Liu, P. Koutrakis, and R. Kahn, "Estimating PM2.5 component concentrations and size distributions using satellite-retrieved fractional aerosol optical depth: Part 1—Development of Methods," *J. Air Waste Manage. Assoc.*, vol. 57, no. 11, pp. 1351–1359, 2007.

[18] Y. Chen, Q. Li, R. A. Kahn, J. T. Randerson, and D. J. Diner, "Quantifying aerosol direct radiative effect with Multiangle Imaging Spectroradiometer observations: Top-of-atmosphere albedo change by aerosols based on land surface types," *J. Geophys. Res.*, vol. 114, p. D02 109, 2009. DOI: 10.1029/2008JD010754.

[19] D. Kim and V. Ramanathan, "Solar radiation budget and radiative forcing due to aerosol and clouds," *J. Geophys. Res.*, vol. 113, p. D02 203, 2008. DOI:10.1029/2007JD008434.

[20] H. Yu, Y. J. Kaufman, M. Chin, G. Feingold, L. A. Remer, T. L. Anderson, Y. Balkanski, N. Bellouin, O. Boucher, S. Christopher, P. DeCola, R. Kahn, D. Koch, N. Loeb, M. S. Reddy, M. Schulz, T. Takemura, and M. Zhou, "A review of measurement-based assessment of aerosol direct radiative effect and forcing," *Atmos. Chem. Phys.*, vol. 6, pp. 613–666, 2006.

[21] J. Zhang and S. Christopher, "Longwave radiative forcing of Saharan dust aerosols estimated from MODIS, MISR, and CERES observations on Terra," *Geophys. Res. Lett.*, vol. 30, no. 23, p. 2188, 2003. DOI:10.1029/2003GL018479.

[22] R. A. Kahn, W.-H. Li, C. Moroney, D. J. Diner, J. V. Martonchik, and E. Fishbein, "Aerosol source plume physical characteristics from space-based multiangle imaging," *J. Geophys. Res.*, vol. 112, no. D11, p. D11 205, 2007. DOI:10.1029/2006JD007647.

[23] L. A. Remer, Y. J. Kaurman, D. Tanre, S. Mattoo, D. A. Chu, J. V. Martins, R.-R. Li, C. Ichoku, R. C. Levy, R. G. Kleidman, T. F. Eck, E. Vermote, and B. N. Holben, "The MODIS aerosol algorithm, products, and validation," *J. Atmos. Sci.*, vol. 62, no. 4, pp. 947–973, Apr. 2005.

[24] Y. J. Kaufman, L. A. Remer, D. Tanré, R.-R. Li, R. Kleidman, S. Mattoo, R. C. Levy, T. F. Eck, B. N. Holben, C. Ichoku, J. V. Martins, and I. Koren, "A critical examination of the residual cloud contamination and diurnal sampling effects on MODIS estimates of aerosol over ocean," *IEEE Trans. Geosci. Remote Sens.*, vol. 43, no. 12, pp. 2886–2897, Dec. 2005.

[25] O. V. Kalashnikova and R. A. Kahn, "Mineral dust plume evolution over the Atlantic from combined MISR/MODIS aerosol retrievals," *J. Geophys. Res.*, vol. 113, p. D24 204, 2008. DOI:10.1029/2008JD010083.

[26] D. J. Diner, J. C. Beckert, T. H. Reilly, C. J. Bruegge, J. E. Conel, R. Kahn, J. V. Martonchik, T. P. Ackerman, R. Davies, S. A. W. Gerstl, H. R. Gordon, J.-P. Muller, R. Myneni, R. J. Sellers, B. Pinty, and M. M. Verstraete, "Multiangle Imaging Spectroradiometer (MISR) description and experiment overview," *IEEE Trans. Geosci. Remote Sens.*, vol. 36, no. 4, pp. 1072–1087, Jul. 1998.

[27] V. M. Jovanovic, S. A. Lewicki, M. M. Smyth, J. Zong, and R. P. Korechoff, *Level 1 Georectification and Registration Algorithm Theoretical Basis*. Pasadena, CA: Jet Propulsion Lab., California Inst. Technol., 1996. JPL D-11532, Rev. B.

[28] D. J. Diner, W. A. Abdou, T. P. Ackerman, K. Crean, H. R. Gordon, R. A. Kahn, J. V. Martonchik, S. R. Paradise, B. Pinty, M. M. Verstraete, M. Wang, and R. A. West, *Multi-angle Imaging SpectroRadiometer Level 2 Aerosol Retrieval Algorithm Theoretical Basis, Revision F*. Pasadena, CA: Jet Propulsion Lab., California Inst. Technol., 2006. JPL D-11400.
[29] M. Bull, J. Matthews, D. McDonald, C. Moroney, S. Paradise, and M. Smyth, *MISR Data Products Specifications, Revision Q*. Pasadena, CA: Jet Propulsion Lab., California Inst. Technol., 2008. JPL D-13963.
[30] G. Zhao and L. Di Girolamo, "A cloud fraction versus view angle technique for automatic in-scene evaluation of the MISR cloud mask," *J. Appl. Meteorol.*, vol. 43, no. 6, pp. 860–869, Jun. 2004.
[31] J. V. Martonchik, D. J. Diner, K. Crean, and M. Bull, "Regional aerosol retrieval results from MISR," *IEEE Trans. Geosci. Remote Sens.*, vol. 40, no. 7, pp. 1520–1531, Jul. 2002.
[32] R. Kahn, P. Banerjee, and D. McDonald, "The sensitivity of multiangle imaging to natural mixtures of aerosols over ocean," *J. Geophys. Res.*, vol. 106, pp. 18 219–18 238, 2001.
[33] L. A. Remer, D. Tanre, Y. J. Kaufman, R. C. Levy, and S. Mattoo, *Algorithm for Remote Sensing of Tropospheric Aerosol From MODIS: Collection 005*, 2009. Revision 2, 89 pp. [Online]. Available: http://modis-atmos.gsfc.nasa.gov/MOD04_L2/index.html
[34] R. C. Levy, R. G. Kleidman, L. A. Remer, C. Ichoku, S. Mattoo, B. N. Holben, and T. Eck, *Global evaluation of the Collection 5 MODIS orbital aerosol products over land and ocean*, 2009. in review.
[35] R. A. Kahn, M. J. Garay, D. L. Nelson, K. K. Yau, M. A. Bull, B. J. Gaitley, J. V. Martonchik, and R. C. Levy, "Satellite-derived aerosol optical depth over dark water from MISR and MODIS: Comparisons with AERONET and implications for climatological studies," *J. Geophys. Res.*, vol. 112, no. D18, p. D18 205, 2007. DOI:10.1029/2006JD008175.
[36] R. A. Kahn, B. J. Gaitley, J. V. Martonchik, D. J. Diner, and B. Holben, "Assessment of MISR global aerosol products," *J. Geophys. Res.*, 2009. to be published.
[37] S. Gassó and A. F. Stein, "Does dust from Patagonia reach the sub-Antarctic Atlantic Ocean?" *Geophys. Res. Lett.*, vol. 34, p. L01 801, 2007. DOI:10.1029/2006GL027693.
[38] L. Liu and M. I. Mishchenko, "Toward unified satellite climatology of aerosol properties: Direct comparisons of advanced level 2 aerosol products," *J. Quant. Spectrosc. Radiat. Transf.*, vol. 109, no. 14, pp. 2376–2385, Sep. 2008.
[39] J. Zhang and J. S. Reid, "MODIS aerosol product analysis for data assimilation: Assessment of over-ocean level 2 aerosol optical thickness retrievals," *J. Geophys. Res*, vol. 111, p. D22 207, 2006. DOI: 10.1029/2005JD006898.

Ralph A. Kahn received the B.S. degree in physics and geology from the University of Rochester, Rochester, NY, in 1973 and the M.S. and Ph.D. degrees in applied physics from Harvard University, Cambridge, MA, in 1975 and 1980, respectively.

He is currently a Senior Research Scientist with the Laboratory for Atmospheres, NASA Goddard Space Flight Center, Greenbelt, MD. He is also Aerosol Scientist for the NASA Earth Observing System's Multi-angle Imaging SpectroRadiometer (MISR). He focuses on using MISR's unique observations, combined with other data and numerical models, to learn about wildfire smoke, desert dust, volcano, and air-pollution particles and to apply the results to regional and global climate-change questions. He has lectured on global climate change and atmospheric physics at the University of California at Los Angeles, and at California Institute of Technology, Pasadena. He is the Editor and Founder of *PUMAS*, the online journal of science and math examples for precollege education (http://pumas.nasa.gov).

David L. Nelson received the M.S. degree in geology from the California Institute of Technology, Pasadena.

He is currently a Senior Data Analyst and Applications Programmer with Raytheon Intelligence and Information Systems, Pasadena, where he has worked with the Multi-angle Imaging SpectroRadiometer (MISR) team for ten years. Among other contributions, he is the principal author of the MINX tool for mapping smoke-plume heights and physical properties from MISR data and has been a lead developer of the MISR Research Aerosol Retrieval Algorithm.

Michael J. Garay received the B.S. degree in physics and the B.A. degree (with honors) in English literature from the University of Toledo, Toledo, OH, in 1995 and the M.S. degree in atmospheric sciences from the University of California at Los Angeles, in 2004.

In 2003, he joined the Multi-angle Imaging SpectroRadiometer (MISR) team at the NASA Jet Propulsion Laboratory, Pasadena, CA, where he is currently a Senior Physics Engineer with Raytheon Intelligence and Information Systems. His research focuses primarily on satellite remote sensing of clouds and aerosols using MISR and other instruments. He has also done work on 3-D radiative transfer, machine-learning techniques for satellite image-feature classification, computer-vision approaches for image-feature tracking, and multidimensional data visualization and analysis for ground-based and satellite systems.

Robert C. Levy received the B.A. degree in mathematics from Oberlin College, Oberlin, OH, in 1994, the M.S. degree in atmospheric science from Colorado State University, Fort Collins, in 1996, and the Ph.D. degree in atmospheric and oceanic science from the University of Maryland, College Park, in 2007.

Since 1998, he has been with the Science Systems and Applications, Inc., Lanham, MD, and he is currently working with the Moderate Resolution Imaging Spectroradiometer (MODIS) aerosol team at the NASA Goddard Space Flight Center, Greenbelt, MD. He is responsible for upkeep, validation, and improvement of the MODIS aerosol algorithms over both land and ocean. In conjunction with his Ph.D. work, he developed a second-generation retrieval algorithm for deriving global aerosol over dark land. He is currently interested in using the MODIS products to study relationships between aerosols, air quality, and climate.

Michael A. Bull received the B.S. degree (with honors) in computer science from the University of Maryland, College Park, in 1992 and the M.S. degree in computer science from the University of California at Los Angeles in 1994.

Since 1996, he has been with the NASA Jet Propulsion Laboratory, Pasadena, CA, where he has been working as a member of the software development team for the Multi-angle Imaging SpectroRadiometer (MISR) project. He is currently providing software-development support for MISR aerosol science algorithms.

David J. Diner received the B.S. degree (with honors) in physics from the State University of New York, Stony Brook, in 1973 and the M.S. and Ph.D. degrees in planetary science from the California Institute of Technology, Pasadena, in 1977 and 1978, respectively.

Since 1978, he has been with the NASA Jet Propulsion Laboratory, Pasadena, where he is currently a Senior Research Scientist with the Science Division. He has been involved in numerous NASA planetary and Earth remote-sensing investigations. He is the Principal Investigator of the Multi-angle Imaging SpectroRadiometer experiment.

Dr. Diner is a member of the American Geophysical Union and the IEEE Geoscience and Remote Sensing Society.

John V. Martonchik received the Ph.D. degree in astronomy from the University of Texas, Austin, in 1974.

In 1972, he joined the NASA Jet Propulsion Laboratory, Pasadena, CA, where he is currently a Research Scientist with the Multiangle Imaging Element of the Earth and Space Sciences Division. He is also the Algorithm Scientist for the EOS MISR Aerosol/Surface product. His experience includes analyzing telescopic and spacecraft observations of planetary atmospheres; laboratory and theoretical studies of the optical properties of gaseous, liquid, and solid materials; and the development and implementation of 1-D and 3-D radiative transfer and line-by-line spectroscopy algorithms for studies of planetary atmospheres and Earth tropospheric remote sensing.

Susan R. Paradise received the B.S. degree in mathematics and computer science from Purdue University, West Lafayette, IN, in 1985 and the M.S. degree in mathematics from the University of Southern California, Los Angeles, in 1992.

In 1985, she joined the NASA Jet Propulsion Laboratory, Pasadena, CA, where she has been working in the area of remote-sensing scientific software development. She has supported the Atmospheric Trace MOlecule Spectroscopy Experiment, Multiangle Imaging SpectroRadiometer (MISR), NASA Earth Observing System's Thermal Emission Spectrometer, and Aerosol Measurement and Processing System (AMAPS) Projects. She is currently serving as a Senior Software and System Engineer for the MISR and AMAPS projects.

Ms. Paradise was the recipient of the NASA Exceptional Service medal for her contributions to MISR in 2002.

Earl G. Hansen received the B.S. degree in mathematics and physics from the University of Washington, Seattle, in 1989.

Since 1972, he has been involved with data system development and operations, including roles as Software Engineer, Systems Programmer, and Systems and Operations Manager with commercial companies and the NASA Jet Propulsion Laboratory (JPL), Pasadena, CA. Since 1989, he has been with JPL, initially as a Systems Engineer for the science data system of the AVIRIS project. In 1992, he became a Senior Systems Engineer and Task Manager for the Science Data System and is currently the Project Manager of the MISR Project.

Lorraine A. Remer received the B.S. degree in atmospheric science from the University of California, Davis, in 1980, the M.S. degree in oceanography from the Scripps Institution of Oceanography, University of California, San Diego, La Jolla, in 1983, and the Ph.D. degree in atmospheric science from the University of California, Davis, in 1991.

In 1991, she came to the NASA Goddard Space Flight Center (GSFC), Greenbelt, MD, employed by the Science Systems and Applications, Inc., until 1998 when she became a civil servant. She is currently a Physical Scientist with the Climate and Radiation Branch of the Laboratory for Atmospheres, GSFC. She is also a member of the EOS Moderate Resolution Imaging Spectroradiometer (MODIS) science team and leads the aerosol subgroup of the Aerosol–Clouds–Ecosystems (ACE) Decadal Survey science working group. Her current research interests include the climatic effects and remote sensing of atmospheric aerosol. She has been involved in several field campaigns including the Smoke/Sulfate, Cloud And Radiation (SCAR) experiments, the Tropospheric Aerosol Radiative Forcing Observational Experiment (TARFOX), the Israeli Desert Transition Zone experiment, the Puerto Rico Dust Experiment (PRiDE), the Chesapeake Lighthouse Airborne Measurements for Satellites (CLAMS), and the Arctic Research of the Composition of the Troposphere from Aircraft and Satellites (ARCTAS).